

The Eocene–Oligocene climate transition in the Central Paratethys

Péter Ozsvárt^{a,*}, László Kocsis^{b,c}, Anita Nyerges^a, Orsolya Györi^d, József Pálfy^{a,e}



^a MTA-MTM-ELTE Research Group for Paleontology, P.O. Box 137, H-1431 Budapest, Hungary

^b Universiti Brunei Darussalam Geology Group, Faculty of Science, UBD-FOS Building, B2.24 Jalan Tungku Link, Gadong BE 1410, Brunei, Darussalam

^c Institute of Earth Science, Faculty of Geosciences and Environment, Géopolis, University of Lausanne, Switzerland

^d MTA-ELTE Geological, Geophysical and Space Science Research Group, Pázmány Péter sétány 1/C, Budapest H-1117, Hungary

^e Department of Physical and Applied Geology, Eötvös Loránd University, Pázmány Péter sétány 1/C, Budapest H-1117, Hungary

ARTICLE INFO

Article history:

Received 8 December 2015

Received in revised form 24 July 2016

Accepted 25 July 2016

Available online 28 July 2016

Keywords:

EOT

Paleogene

Climate evolution

$\delta^{18}\text{O}$ and $\delta^{13}\text{C}$ records

Paleoceanography

Foraminifera

Calcareous nannoplankton

ABSTRACT

We studied two boreholes (Cserépváralja-1 and Kiscell-1) with continuous sedimentary records across the Eocene–Oligocene climate transition from the Central Paratethyan area. Assemblages of benthic foraminifera display a shift in dominance by epifaunal taxa in the late Eocene to shallow and deep infaunal taxa in the early Oligocene. Using the benthic foraminiferal oxygen index (BFOL), a decreasing trend of bottom-water oxygen levels is established across the Eocene–Oligocene transition (EOT), leading to the development of dysoxic conditions later in the early Oligocene.

Trends in $\delta^{18}\text{O}$ and $\delta^{13}\text{C}$ values measured on tests of selected benthic and planktic foraminifera roughly parallel those of the global record of stepped EOT $\delta^{18}\text{O}$ increase and deviate only later in the early Oligocene, related to the isolation of the Paratethys. The overall similarity of the isotope curves and the presence of a planktic–benthic ecological offset suggest that the original isotope trends are preserved, despite the systematically more negative $\delta^{18}\text{O}$ values. Of different scenarios, a quasi-uniform diagenetic overprint by fluids with low $\delta^{18}\text{O}$ values, during burial or uplift, appears best supported. We conclude that the globally established isotopic expression of Antarctic ice sheet growth across the EOT may be recognizable in the Paratethys. Deviations from the global trends after the EOT were caused by regional paleoceanographic changes induced by the progressing Alpine orogeny and sea-level change, which led to a restricted connection with the open ocean, freshwater influx from increased precipitation, and gradual development of bottom-water oxygen depletion.

© 2016 Elsevier B.V. All rights reserved.

1. Introduction

The onset of major Antarctic glaciation close to the Eocene–Oligocene boundary was one of the most significant events in the climate evolution of the Cenozoic Era. The principal cause of this climate transition is debated, although its consequences are indisputable: rapid expansion of continental ice volume on Antarctica (e.g., Shackleton and Kennett, 1975; Miller et al., 1991; Zachos et al., 1996; Lear et al., 2008; Galeotti et al., 2016) and significant (> 1 km) deepening of the global calcite compensation depth (e.g., Coxall et al., 2005) from ~34 Ma. A remarkable decrease in atmospheric $p\text{CO}_2$ is also detected (e.g., Pagani et al., 2005; DeConto et al., 2007; Pearson et al., 2009) during the Eocene–Oligocene transition (EOT), although the exact magnitude of change is still poorly defined. All inferences are derived from deep-sea benthic foraminiferal oxygen and carbon isotope ($\delta^{18}\text{O}$, $\delta^{13}\text{C}$) records, which have been extensively studied, on the basis of the vast amount of Deep Sea Drilling Project (DSDP), Ocean Drilling Program (ODP) and Integrated Ocean Discovery Program (IODP) cores (e.g., Shackleton and Kennett, 1975; Zachos et al., 1996, 2001; Salamy and Zachos, 1999; Coxall et al., 2005; Pearson et al.,

2009). However, significantly fewer studies have focused on the record of isolated marginal seas or terrestrial paleoclimatic changes from this interval (e.g., Zanazzi et al., 2007; Kocsis et al., 2014). The stratigraphic record of marginal seas, such as the Paratethys in east-central Europe, may provide valuable new insights about the EOT, but the scarcity of available stable isotope data has hampered the understanding of this dramatic climate change event in this area. Moreover, the northward drift and rotation of the African continent and related microcontinents (e.g., the Apulian microcontinent) and their collision with the European foreland had a strong impact on Cenozoic paleoceanography, paleogeography and paleoclimate (Kocsis et al., 2014). The ongoing subduction of the Eastern Alps and external Carpathian lithosphere under the overthrust Apulian units (Csontos et al., 1992) resulted in the first isolation of Paratethys from the late Eocene (e.g., Báldi, 1984; Rögl, 1998). However, seaways existed intermittently between the North Sea and the Paratethys, and the repeated disconnections of the Paratethys from the adjacent oceans eventually led its isolation by the late early Oligocene. Increased river runoff from surrounding landmasses resulted at times in a strongly stratified water column and dysoxic to anoxic conditions in the moderately deep-water Paratethyan subbasins (Báldi, 1984). Regional tectonic activity and significant glacio-eustatic fluctuations during the early Oligocene might have reduced the surface and bottom water mass

* Corresponding author.

E-mail address: ozsi@nhmus.hu (P. Ozsvárt).

exchange between the Paratethys, the western part of Neotethyan basin, and the Atlantic Ocean, which in turn could have restricted the internal circulation pattern within the Paratethys. These oceanographic changes led to repeated deposition of laminated organic-rich sediments, considered as hydrocarbon source rocks from the Alpine molasse basins through the Central Paratethys (Hungarian Paleogene Basin (HPB), Slovenian Paleogene Basin, Central Carpathian Paleogene Basin and Transylvanian Paleogene Basin) to the Caucasus (Báldi, 1984). The paleoenvironmental consequences of the progressive separation of the Paratethys are reflected in radical changes in numerous marine proxies that imply unstable paleoceanographic conditions. The causes and consequences of these paleoenvironmental changes during the EOT are still not fully understood. The primary objective of this study is to reconstruct the paleoclimatic and paleoceanographic changes of the Central Paratethys during the EOT. Two continuous epicontinental Eocene/Oligocene boundary core sections (Cserépváralfa-1 [CSV-1] and Kiscell-1 [KL-1]) from the HPB of the Central Paratethys have been investigated, including studies of their foraminifera and calcareous nannoplankton and high-resolution stable isotope geochemical analyses, which allowed paleoecological and paleoceanographic reconstructions. Comparison of the results is then used to assess whether the well-dated global paleoclimatic signals can be recognized in the regional climate archive of the Paratethys.

2. Geological setting and stratigraphy

The Hungarian Paleogene Basin (HPB) is one of the largest Paleogene basin remnants in the Eastern Alpine–Western Carpathian–Dinarides junction (Fig. 1) and includes various subbasins, which contain different sedimentary successions. Several tectonic models have been proposed in order to explain the evolution of HPB (Báldi and Báldi-Beke, 1985;

Báldi-Beke and Báldi, 1991; Csontos et al., 1992; Tari et al., 1993, Kázmér et al., 2003). One of their common features is that they attempt to relate the basin-forming mechanisms to strike-slip tectonics and an overall ENE-directed migration of subsequent depocenters (Tari et al., 1993). Owing to the economic interest and exploration for coal, bauxite, and hydrocarbon, thousands of industrial wells provide scientific information about the middle Eocene to upper Oligocene succession in the region. In the central part of the HPB the Paleogene sedimentation started in the late Eocene (NP18) with a typical transgressive succession (Vörös, 1989). The sedimentary succession is the following: terrestrial clastic rocks with coal measures followed by shallow marine carbonates, and a transgressive succession of dark shale or bryozoan marl overlain by shallow bathyal marl (Buda Marl Formation), which upwards continuously grades into anoxic black shale (Tard Clay Formation). This continuous shallow bathyal succession with water depths between ~500 and 800 m contains the EOT in the HPB, including clay, siltstone, marl, shallow-water limestone, clayey marl, argillaceous siltstone and shale (Báldi, 1986). Water-depth reconstructions are based on quantitative analysis of benthic foraminifera assemblage and planktic/benthic foraminiferal ratios (Ozsvárt, 2007). The Tard Clay Formation was deposited under dominantly anoxic conditions in a sediment-starved basin (Báldi et al., 1984), where sedimentation rate was extremely low ($30\text{--}50\text{ m Myr}^{-1}$). In the anoxic, laminated black shale, mono- or duospecific calcareous nannoplankton assemblages occur, suggesting brackish surface-water conditions (Nagyvarosy, 1985). Similar anoxic black shales are common in the Alpine foreland, in the Carpathian Flysch belt and in the Transylvanian Paleogene Basins as well (Fig. 1), indicating the first isolation of the Paratethys from the westernmost part of the Neotethys Ocean (Fig. 2). The laminated strata gradually pass upward into argillaceous siltstone and clay (Kiscell Clay Formation), with the simultaneous appearance of a diverse benthic and planktic

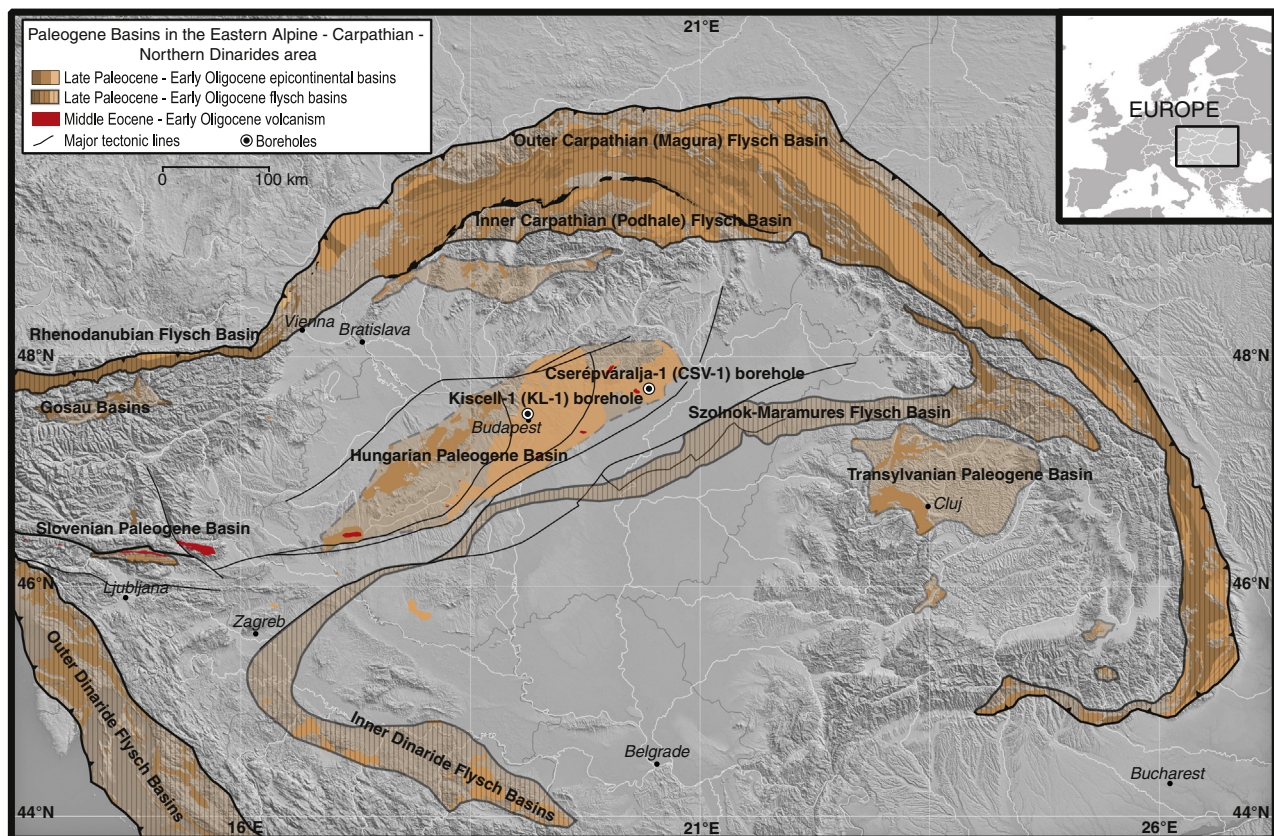


Fig. 1. Paleogene epicontinental and flysch basins in the Eastern Alpine–Carpathian–Northern Dinarides junction. Map showing the location of the Cserépváralfa-1 (CSV-1) and Kiscell-1 (KL-1) boreholes. Base map derived from the digital elevation model of the Pannonian Basin (Horváth et al., 2005).

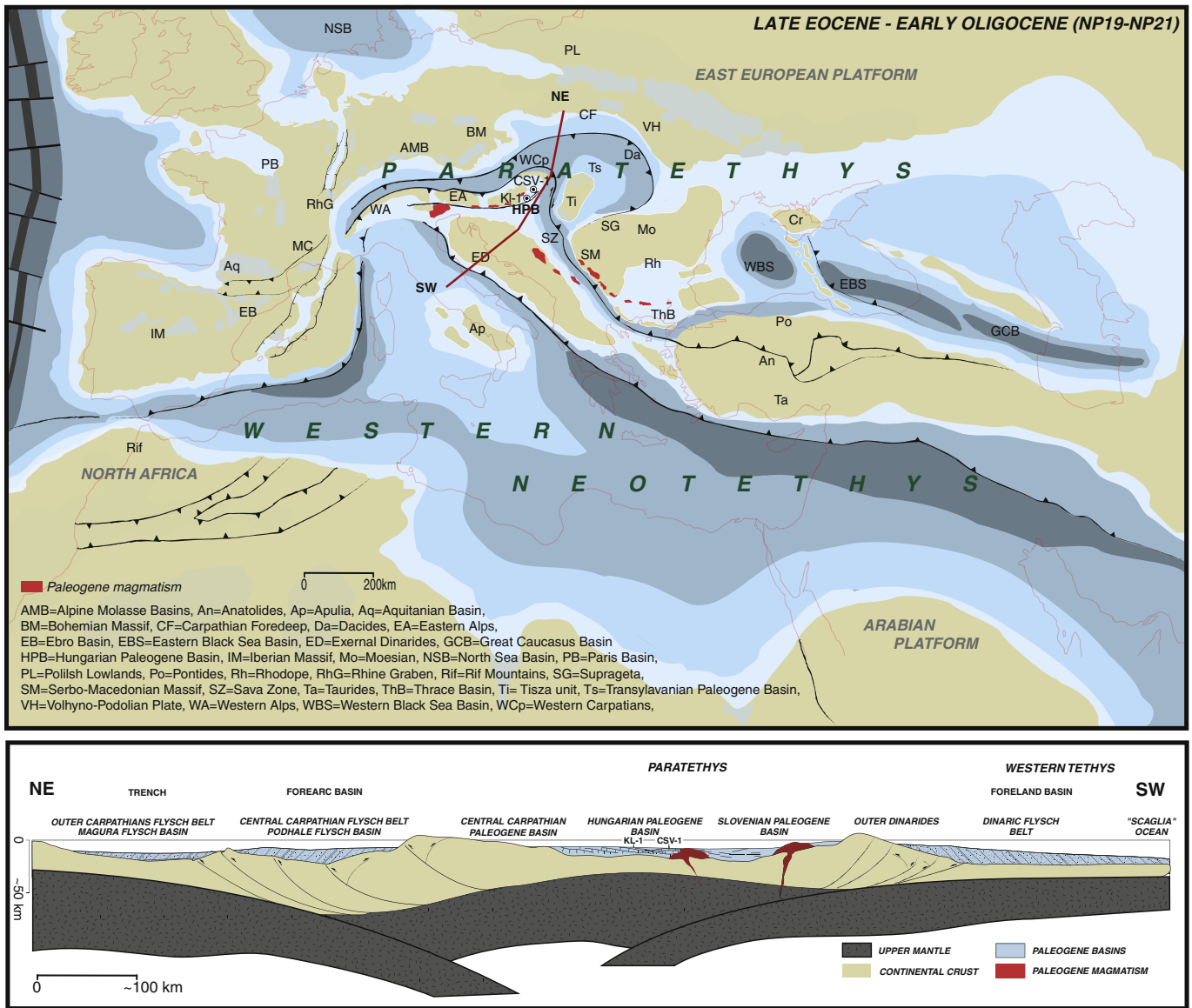


Fig. 2. Paleogeographic reconstruction of the Alpine-Carpathian-Dinarides junction for Eocene-Oligocene transition (NP19-NP21), based on paleogeographic maps of Ziegler (1990), Dercourt et al. (1993), Rögl (1998), Meulenkamp and Sissingh (2003) and Popov et al. (2004). The tectonic cross-section is based on Tari et al. (1993).

fauna that implies the return of normal marine conditions and re-established connection to the open ocean (Báldi et al., 1984).

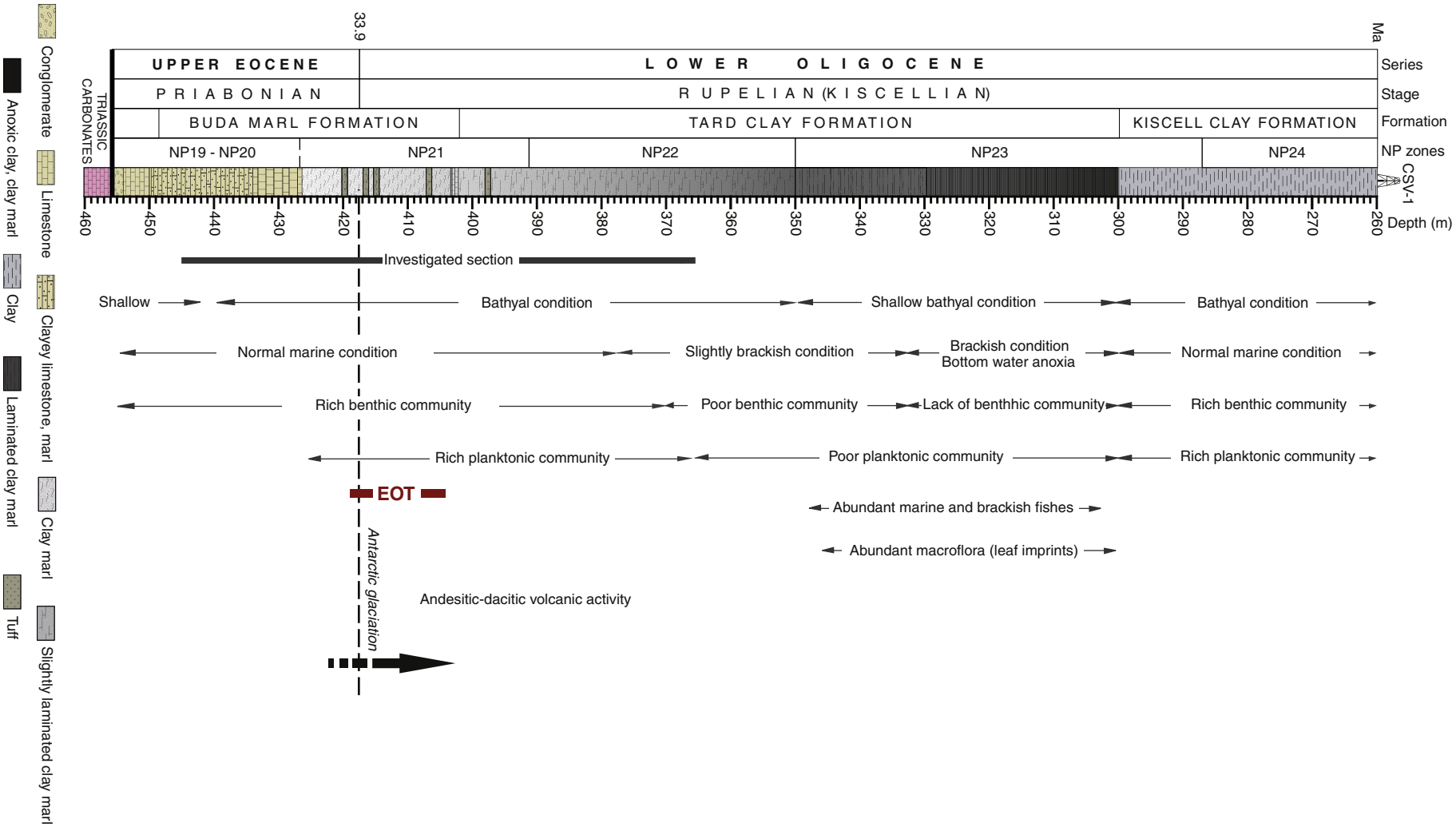
2.1. EOT strata in the CSV-1 borehole

The CSV-1 hydrocarbon exploration borehole was drilled in 1977 in the southern foreland of Bükk Mts. in Northeastern Hungary (Fig. 1). The borehole penetrated ~460 m of sediments, of which EOT strata were recovered in ~100 m thickness (Fig. 3). Unpublished sedimentological and geophysical measurements from CSV-1 borehole are available in the archive of the Geological and Geophysical Institute of Hungary (MFGI). The entire CSV-1 core is archived in the core repository of the MFGI at Rákóczi tép, Hungary. All investigated samples are housed in the Department of Paleontology and Geology of the Hungarian Natural History Museum, Budapest. The transgressive upper Eocene (NP20) conglomerate and carbonate (Szépvölgy Limestone Formation) grade at a depth of 426.3 m into grey (Fig. 3), greenish grey marl (Buda Marl Formation). Upwards, between 402.0 and 350.0 m, the carbonate content decreases, while the clay content increases and the succession becomes lithologically more homogenous in the lower member of

Tard Clay Formation (Fig. 3). This unit is non-laminated siltstone with characteristic marine micro and macrofauna (Bechtel et al., 2012). Between 350.0 and ~300 m thin-bedded, slightly laminated, dark brownish siltstone occurs, which is grading continuously upward into anoxic (Fig. 3), dark brownish grey shale with up to 5 wt.% TOC, alternating locally with thin, white coccolith-bearing layers (Nagymarosy, 1985). The anoxic black shale is followed by shallow bathyal, brownish grey argillaceous, calcareous siltstone, claymarl and sandstone (Kiscell Clay Formation). For the present study, the upper Eocene and lower Oligocene section were sampled between 443.1 and 364.0 m (see Fig. 3). The preservation of planktic and benthic foraminifera is moderate to excellent.

2.2. EOT strata in the KL-1 borehole

The KL-1 borehole was drilled in 1980, in the northwestern part of Budapest (Fig. 1) and it penetrated ~96 m thick EOT strata (Fig. 4). This is the most comprehensively studied Eocene-Oligocene section from the Paratethys with biostratigraphic (nannoplankton and planktonic foraminifera), magnetostratigraphic, and K/Ar radiometric data



(Báldi, 1984). The KL-1 section is the lower boundary stratotype of the regional lower Oligocene Kiscellian Stage. The core is housed in the core repository of MFGI in Szépvízér, Hungary. The sediments consist of mainly grey and greenish grey marl (Buda Marl Formation) between 110 m and 91.4 m (Fig. 4) and dark grey, non-laminated and strongly laminated claystone (Tard Clay Formation) between 91.4 m and 14.0 m (Fig. 4). The Buda Marl and Tard Clay formations display a gradational transition without any major changes in the sedimentation during the EOT, with characteristic benthic foraminiferal assemblages. A significant change can be observed at about 65 m (Fig. 4), where the non-laminated strata pass upward into dark grey, brownish, slightly laminated member of Tard Clay Formation. A typical cold-adapted epiplanktic mollusc fauna (*Spiratella* spp.) appears around 70 m and indicates the increasing influence of cold water masses (Báldi, 1984). Between 52 and 14 m thin-bedded or laminated, dark grey to black shale occurs (Fig. 4), suggesting deposition under anoxic conditions. The carbonate content is around 50 wt.% in the lower part of the core and it decreases to 10 wt.% in the upper, strongly laminated part (Kázmér, 1985), which indicates decreasing carbonate production parallel to the development of anoxic environment. The upper Eocene and lower Oligocene parts of the section were sampled between 107.4 and 69.8 m (Fig. 4) for this study. The preservation of planktic and benthic foraminifera is moderate.

2.3. Eocene-Oligocene biochronology of the boreholes

For biostratigraphy of the Paleogene formations in Hungary, the standard nannoplankton zonation of Martini (1970) was used (Báldi-Beke, 1972, 1977, 1984; Báldi et al., 1984; Nagymarosy and Báldi-Beke, 1988). In this study, either all of the species present or the more commonly occurring ones were considered for the definition of zone boundaries (see Supplementary Material 1). The preservation of zonal marker species of EOT is generally good, but because of the rare occurrence of the tropical forms, some of the zonal markers of Martini (1970) need to be substituted with locally important species of the genera *Sphenolithus*, *Ericsonia*, *Reticulofenestra* and *Helicosphaera*. Due to their small size, coccoliths can be easily reworked but it does not affect their usefulness as age indicators in this study.

The Buda Marl Formation represents the NP20 and lower part of the NP21 zone, whereas the overlying Tard Clay Formation represents the upper part of the NP21 zone and the NP22–NP23 zones (see Supplementary Material 1). Nyerges (2014) drew the boundary between zones NP20 and NP21 at 427.7 m in the CSV-1 borehole (Fig. 3). In the KL-1 borehole, the Eocene-Oligocene boundary lies approximately at 90 m (Fig. 4), between the P17 and P18 planktic foraminifera zones and within the NP21 nannozone (Báldi, 1984). The boundary between zones NP21 and NP22 was drawn at 391 m in the CSV-1 borehole (Fig. 3) and at 78 m in the KL-1 borehole (Fig. 4). The ratified global Eocene/Oligocene boundary was defined in the middle part of the NP21 zone, on the basis of the extinction of two planktic foraminifera genera (*Hantkenina* and *Cribohantkenina*) at the boundary of P17 and P18 planktic foraminifera zones (Premoli Silva and Jenkins, 1993). In the international nannoplankton zonation, NP21 straddles the Eocene-Oligocene boundary (Martini, 1971), but the exact position of the series boundary cannot be defined by nannoplankton data alone. Due to the absence of the late Eocene *Hantkeninidae* from the HPB, the Eocene/Oligocene boundary in the CSV-1 borehole was approximated by the last appearance (LAD) of *Subbotina linaperta* and the first appearance (FAD) of *Pseudohastigerina naguwichiensis* and *Chiloguembelina gracillima* within the middle part of NP21 (Báldi et al., 1984).

3. Material and methods

3.1. Sample preparation and benthic foraminifera assemblage analysis

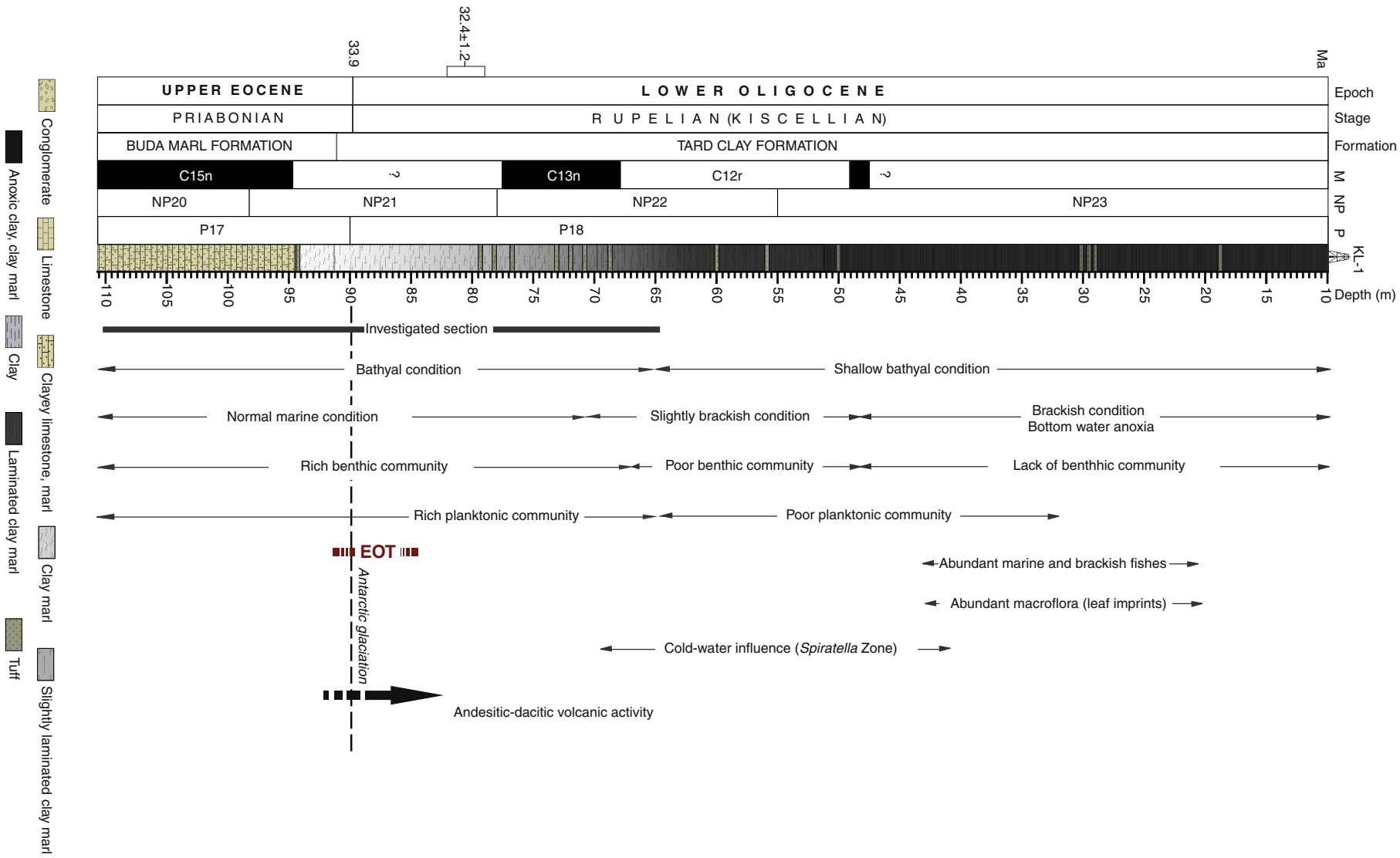
Approximately 250–300 g from each core sample was processed for the benthic foraminiferal studies. Samples were dried, weighed and disaggregated with 10% H₂O₂ in an ultrasonic bath and washed with distilled water. No oxide coating was visible on any of the samples. The residues were washed through a 50- μ m sieve and dried. Samples were divided into grain-size fractions of 50–500 μ m and >500 μ m. Faunal analysis was performed only on the 50–500 μ m fraction. For faunal analysis, ~200–250 specimens were picked, unless their numbers were <200, in which case all specimens were picked. Species occurrence and abundance distribution data (Supplementary Material 2) were used to calculate the Shannon-Wiener diversity H(S) index and to perform Q-mode (Varimax-rotated) principal factor analysis. The Shannon-Wiener diversity H(S) index was calculated in order to estimate the stability of benthic foraminiferal community (Buzas and Gibson, 1969). We distinguished foraminiferal associations by Q-mode principal factor analysis with subsequent Varimax rotation (for details see Vető et al., 2007). The statistics software package SYSTAT 13 was used for statistical calculations.

3.2. Benthic foraminiferal oxygen index (BFOI)

In the last decades, a number of studies documented that skeleton morphology of benthic foraminifera is strongly related to microhabitat preferences (e.g. Corliss, 1991; Jorissen et al., 1995; Vető et al., 2007). These different benthic environments are strongly controlled by organic carbon flux and dissolved oxygen content at the sediment–water interface and in the uppermost few centimeters of the sediment (e.g., Mackensen et al., 1985; Schmiedl et al., 1997). We used the BFOI in order to estimate changes in bottom-water oxygenation. This index was calculated using Kaiho's empirical equations for dissolved oxygen content in bottom water, on the basis of a global database of modern assemblages (Kaiho, 1994). The BFOI reflects the estimated dissolved oxygen levels in modern ocean waters, which is based on the proportion of forms with different microhabitat preference among the benthic foraminifera. As an extension of his method, Kaiho (1994) successfully used the dissimilarity of benthic foraminiferal test morphology to extrapolate relative amounts of dissolved oxygen in the world oceans from early Eocene to late Oligocene times.

3.3. Stable oxygen and carbon isotopes

Stable isotope analyses ($\delta^{18}\text{O}$, $\delta^{13}\text{C}$) were carried out on foraminifera tests and used together with quantitative paleontological methods for paleoecological and paleoceanographical inferences. *Cibicides* spp. (including its most abundant species, *C. dutemplei*) were chosen in all except for two samples, where their absence or poor preservation forced us to pick another species, *Gyroidinoides soldanii* (see Supplementary Material 3 for details). Among planktic foraminifera, the same species of Globigerinida (*Globigerinida* sp. 2) were selected from both sites for stable isotope analysis. The tests of foraminifera were directly analyzed using a Gasbench II coupled to a Finnigan MAT Delta Plus XL mass spectrometer at the Stable Isotope Laboratory of the Institute of Earth Sciences at University of Lausanne, Switzerland. The methods used are described in detail in Spötl and Vennemann (2003). Every sample from the CSV-1 borehole was measured in duplicates, whereas single samples were measured from the KL-1 borehole. The analytical precision was better than $\pm 0.1\%$ for O and C isotopes. Oxygen and carbon isotope compositions are expressed in the δ -notation relative to VPDB (Vienna Pee Dee Belemnite).



3.4. Assessing diagenetic effects on the foraminifera tests

In order to assess possible diagenetic recrystallization, scanning electron microscopic images of the foraminifera tests were analyzed. A Hitachi S-2600N scanning electron microscope operated at 25 kV and 15–20 mm distance was used. To study the infill of the tests, 40- μ m-thick equatorial thin sections were prepared and the polished sections were examined by a MAAS-Nuclide ELM-3 cold-cathode luminoscope at the Department of Physical and Applied Geology of the Eötvös Loránd University.

3.5. Nannoplankton analysis

The calcareous nannoplankton flora of the CSV-1 borehole was previously studied at a much lower resolution, with sample spacing of 6 m (Báldi et al., 1984). Here a sample spacing of 20 cm was used to obtain a total of 108 smear slides to study calcareous nannoplankton assemblages. Slide preparation followed the standard techniques (Bown, 1998), which are known to retain the original composition of the nannoplankton assemblages of the sediments. More than 57,000 specimens were determined at the species level whenever possible, by viewing at least 30 fields of view per slide and counting all the observed specimens (see Supplementary Material 4). Following the identification, a quantitative analysis of the nannoplankton flora was performed using diversity indices and multivariate data analysis, including cluster analysis and detrended correspondence analysis (DCA), using the PAST software package (Hammer et al., 2001).

4. Results

4.1. Benthic foraminiferal analyses

Investigation of the tests by stereomicroscope revealed that most of the foraminifera tests are frosty-opaque in appearance (Sexton et al., 2006), although glassy specimens were found as well. For stable isotope analysis the least frosty tests were selected. SEM analyses demonstrate that most of the shells are pristine in both investigated assemblages, and only very few have calcite overgrowths (Fig. 5A and B). Thin sections prepared from the tests show very finely to finely crystalline calcite cement (Fig. 5C) and/or pyrite filling the chambers. The calcite exhibits bright orange cathodoluminescence (CL) (Fig. 5D).

The benthic foraminifera assemblages of both studied sections are dominated by epifaunal genera (e.g., *Cibicidoides*, *Gyroidinoides*) in the lower part (between 443.1 m and 404.5 m at CSV-1 site and between 107.4 m and 96.6 m at KL-1 site). Upsection (between 404.2 and 364.0 m in CSV-1 and between 96.2 m and 69.8 m in KL-1) the assemblage is characterized by shallow to deep infaunal genera (e.g., *Lenticulina*, *Bulimina*, *Uvigerina*, *Dentalina*).

A total of 236 foraminifera species were identified in this study. The most characteristic taxa, i.e. those determined as dominant elements of the successive communities distinguished on the basis of factor analysis (see 4.3.) are briefly described and illustrated in Supplementary Material 3.

4.2. Diversity $H(S)$

Benthic foraminiferal diversity index values vary between 1.5 and 3.5 in both studied boreholes. The diversity is slightly increasing in the lower part of CSV-1 core (Fig. 6), whereas it exhibits more or less constant values in the KL-1 core (Fig. 7). A significant increase of diversity index values was observed in the middle part of CSV-1 core (between 425 m and 380 m), whereas strong fluctuation of $H(S)$ values (between 1 and 3) characterizes the middle part of KL-1 core (between 100 m and

80 m). The $H(S)$ values show significant decrease in the upper part of both successions.

4.3. Q-mode factor analysis

Based on the Q-mode factor analysis, the late Eocene–early Oligocene benthic foraminiferal assemblages were grouped into five factor communities in both boreholes (Figs. 6 and 7). In the CSV-1 core, the five factors explain 71.7% of the total variance, whereas in the KL-1 core these factors explain 72.7% of the total variance. *Cibicidoides dutemplei* is the dominant species (factor score 11.38 in CSV-1 core and 7.7 in KL-1 core) in the factor community 1 (FC-1) in both boreholes. Important associated species (i.e. factor score > 1) of this fauna include *Gyroidinoides soldanii* (in both cores), *Spiroplectammina carinata* and *Lenticulina arcuatostrata* (in CSV-1 only). This community occurs between 443.1 m and 404.5 m in the CSV-1 core and between 106.56 m and 96.6 m in the KL-1 core. The FC-2 (*Uvigerina coccaensis jacksonensis*) together with FC-4 (*Bathysiphon saidi* associated with *Clavulinoides szaboi*, *G. soldanii* and *Lenticulina inornata*) show statistically significant factor loadings between 405 m and 388.7 m in the CSV-1 borehole. A similar community (*C. szaboi*, *Dentalina budensis* and *B. saidi*) is dominant in the KL-1 borehole between 96 m and 92 m. Significant loadings of the FC-3 occur between 380 m and 370 m in the CSV-1 borehole, where the dominant species is the infaunal *Cyclammina acutidorsata*. The FC-3 (*Glandulina reussi*, *Dorothia textilaroides*, *Anomalinooides alazanensis*), FC-5 (*Bulimina* spp.) and FC-2 (*L. inornata*) are dominant in the middle part (between 93 m and 79 m) of the KL-1 borehole. The uppermost part between 370 and 364 m is characterized by FC-5 (*L. inornata*, *Cancriis* sp. and *Spiroplectammina carinata*) in CSV-1, and FC-2 (*L. inornata*) in KL-1 (between 77 m and 70 m).

4.4. Benthic foraminiferal oxygen index (BFOI)

The calculated BFOI values range between 0 and 85 in both boreholes, and changes in both curves are characterized by a gradual decrease upsection (Figs. 6 and 7). In the CSV-1 core, relatively high BFOI values (>50) were recorded in the lower part (443.1–409.9 m), similarly to the lower part (107–97 m) of the KL-1 core. The estimated O_2 concentration in bottom-water was higher than 3 ml/l at both sites during deposition of the lower part of the section, which is characterized by the epifaunal *Cibicidoides dutemplei* assemblage (FC-1) and associated epifaunal and shallow infaunal species (*Gyroidinoides soldanii*, *Spiroplectammina carinata* and *Lenticulina arcuatostrata*). In the middle part of both cores (~410–393 m in CSV-1 and ~96–78 m in KL-1), the BFOI values drop below 50 ($15 < \text{BFOI} < 50$), indicating decreasing oxygenation of the depositional environment (Figs. 6 and 7), where the estimated O_2 concentration of the bottom-water ranged between 1.5 and 3.0 ml/l. This interval is characterized by the infaunal *Uvigerina coccaensis jacksonensis* (FC-2) and *Bathysiphon saidi* (FC-4) assemblages, associated with shallow infaunal and epifaunal forms (*Clavulinoides szaboi*, *Gyroidinoides soldanii* and *Lenticulina inornata*) in CSV-1 core (Fig. 6). In the KL-1 core (~96–78 m) it is dominated by infaunal agglutinated foraminifera, *C. szaboi* (FC-4) and associated species (*Dentalina budensis* and *B. saidi*). This part is further characterized by the *Glandulina reussi* (FC-3), *Lenticulina inornata* (FC-2) and *Bulimina truncana* assemblages (FC-5), which are dominated by shallow and deep infaunal species (Fig. 7). In the uppermost part of the cores (above 380 m in CSV-1 and 78 m in KL-1, see Figs. 6 and 7), the BFOI drops to the lowest values (0–15) within the entire investigated part of both boreholes, indicating suboxic conditions with ca. 0.3–1.5 ml/l dissolved oxygen content in the bottom-waters. This interval is characterized by *Cyclammina acutidorsata* (FC-3) and *Lenticulina inornata*

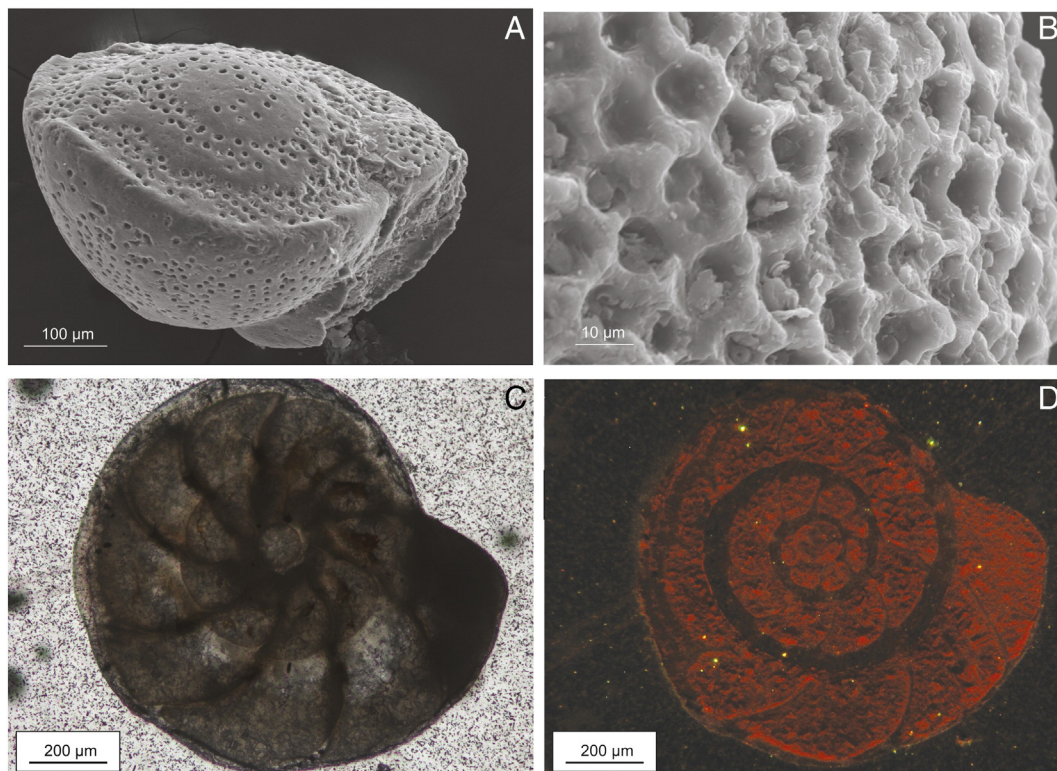


Fig. 5. A) SEM-SE images of a benthic foraminifera (*Cibicidoides dutemplei*, CSV-1 core, 382.2 m), showing pristine shell structure, B) SEM-SE image of the test of a planktic foraminifera from the CSV-1 core, showing minimal calcite overgrowth, C) photomicrograph of a benthic foraminifera (*C. dutemplei*) in thin section (plane-polarized light). Note the distinction between the test wall and the calcite cement filling of the chambers, D) cathodoluminescence image of *C. dutemplei*, note bright orange CL of the calcite cement.

assemblages (FC-5) with associated infaunal species (Fig. 6) in the CSV-1 core, and *Lenticulina inornata* assemblages (FC-2) in the KL-1 core (Fig. 7).

4.5. Calcareous nannoplankton of CSV-1 core

The distribution and association of nannoplankton species primarily depend on temperature, salinity and the availability of nutrients. Báldi-Beke (1984) was the first to distinguish groups in the Hungarian Eocene assemblages on the basis of similar ecological requirements. Following her studies, the principal works about coccolithophores by Bukry (1974), Perch-Nielsen (1985), Winter and Siesser (1994), Bown (1998) and Thierstein and Young (2004), as well as comparative studies by Persico and Villa (2004), Dunkley Jones et al. (2008), Maravelis and Zeligidis (2012), and Violanti et al. (2013) are used here. Nannoplankton occurrence and abundance distribution in the CSV-1 borehole (Supplementary Material 4) was analyzed by constructing diversity curves and carrying out multivariate analyses (Nyerges, 2014). On this basis, the following revised ecological groups are distinguished in the studied material.

4.5.1. Pelagic, normal-salinity nannoplankton association

Characteristic taxa include *Discoaster barbadiensis*, *D. saipanensis*, *D. tani*, *Sphenolithus moriformis*, *S. predistentus*. Others with similar ecological requirements are *Reticulofenestra reticulata*, *R. hampdenensis*, *R. callida*, and *R. minuta*. They are interpreted as open-marine, oceanic forms, preferring mainly tropical-subtropical climate. In the Central Paratethys, they are typical in the Buda Marl Formation, which was deposited at times of fully open marine connection. The other assemblage from similar habitat shows lower diversity; its characteristic taxa include *Reticulofenestra bisecta*, *Blackites tenuis*, *Coccolithus pelagicus*, and *C. floridanus*. These taxa are also interpreted to occupy open-marine habitats, although preferring mainly temperate or cool climate.

4.5.2. Nearshore nannoplankton association

Dominant taxa include *Helicosphaera euphratis*, *H. intermedia*, *Pontosphaera multipora* and *Transversopontis pulcher*, preferring mainly cool climate. Also assigned to this subgroup is the association of the following taxa, which can be linked to the early Oligocene climate cooling: *Lanternithus minutus*, *Zygrhablithus bijugatus*, *Ericsonia subdisticha* and *E. formosus*. Multivariate statistical analyses suggest that *Isthmolithus recurvus* is also related to this group. *Braarudosphaera bigelowii*, *Helicosphaera* sp. and *Transversopontis pulcher* are additional typical species of the inferred nearshore habitat which are able to tolerate reduced salinity. Taxa adapted to warm climate became extinct or ceased to secrete calcareous test at the end of the NP19-20 zone. Upwards the cold-adapted species become dominant, marked by the acme of *Lanternithus minutus*, *Zygrhablithus bijugatus*, and *Ericsonia subdisticha* in the NP21 zone. At the boundary of NP21 and 22 zones the abundance of *Helicosphaera* increases further, showing a trend opposite to all other taxa. *Helicosphaera* is thought to tolerate decreasing salinity and increase in terrestrial influx (Thierstein and Young, 2004; Violanti et al., 2013). In the studied interval the abundance of calcareous nannoplankton is high whereas their preservation is moderate to good. Based on diversity indices (Shannon, Fisher-alpha, evenness, dominance), the nannoflora is highly diverse, rich in taxa, it has moderate evenness and more than one species show relatively high abundance (Fig. 8). The calcareous nannoflora of KL-1 core was not restudied here, but it is known to range from the NP19-20 to NP23 zones (Báldi, 1984).

4.6. Oxygen and carbon isotope analyses

The $\delta^{18}\text{O}$ values vary between -5.9 and -1.6‰ in the entire CSV-1 core, with clearly identifiable trends over time: in the late Eocene to early Oligocene (433.5–404.8 m) the $\delta^{18}\text{O}$ curve shows a significant overall increase with stepped fluctuations (Fig. 9A). The first increase in benthic foraminiferal $\delta^{18}\text{O}$ starts at 425.9 m, the next one at

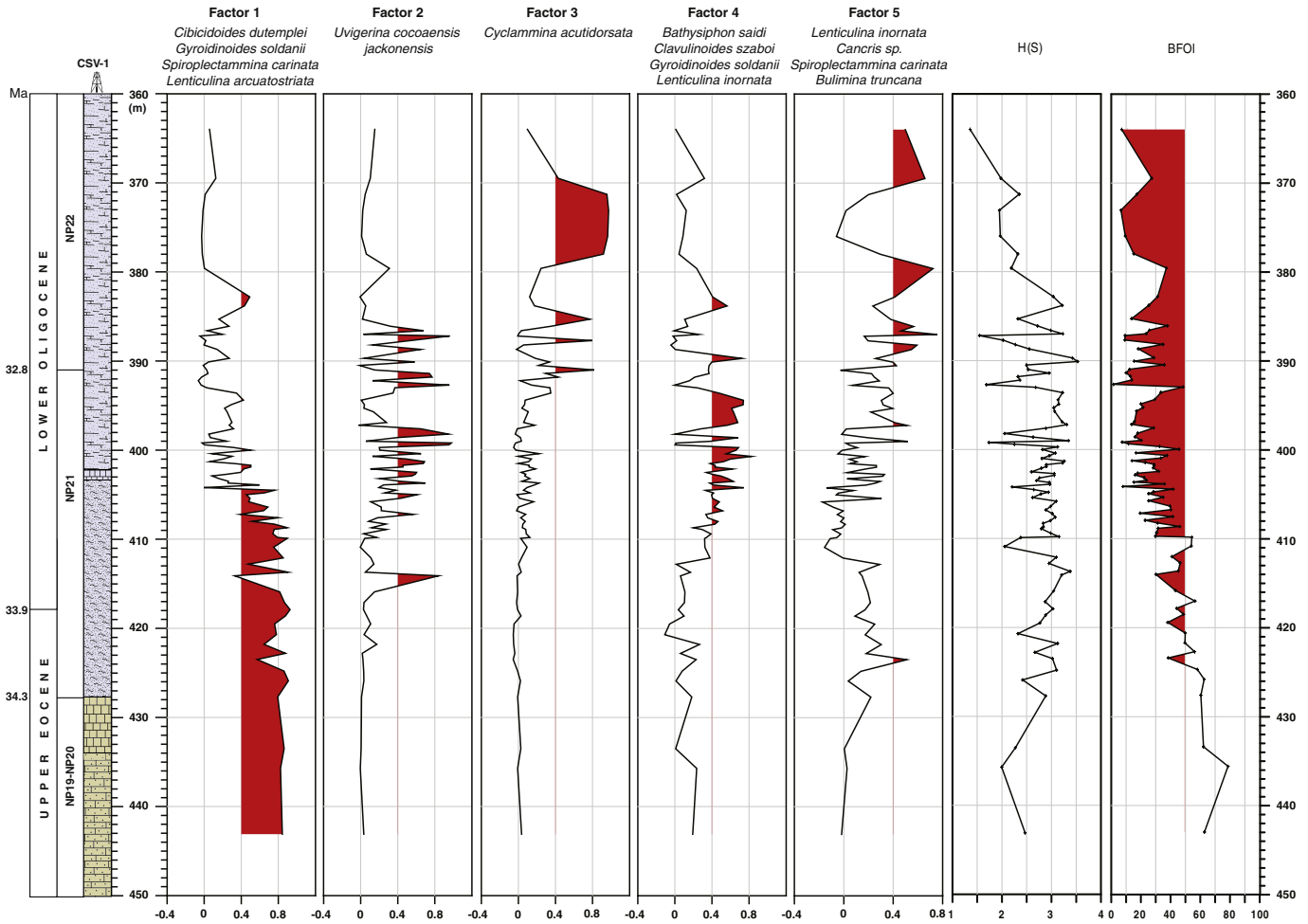


Fig. 6. Q-mode (Varimax-rotated) factor analysis, Diversity H(S) and benthic foraminiferal oxygen index (BFOI) vs. depth in the CSV-1 borehole.

419.5 m, and the most significant one at 404.8 m. The last step leads to the maximum value observed in the oxygen isotope curve (Fig. 9A). Above this interval, the $\delta^{18}\text{O}$ values decrease to 385.3 m, whereas a significant scatter is observed in the uppermost part of the succession. In the KL-1 core, the benthic foraminifera $\delta^{18}\text{O}$ signal (Fig. 9B) shows similar trends to that observed in CSV-1 borehole. The $\delta^{18}\text{O}$ values range from -5.4 to -0.9‰ , with a gradual increase from the lower part of the section to 83 m where they reach the maximum values (Fig. 9B). The trend becomes negative upsection, although a reversal occurs at the uppermost part in KL-1.

The planktic $\delta^{18}\text{O}$ curves show a very similar trend to the $\delta^{18}\text{O}$ curve of benthic foraminifera from both cores, although with more negative $\delta^{18}\text{O}$ values ranging from -6.3 to -3.8‰ in the CSV-1 core and -5.9 to -2.3‰ in KL-1. The average observed surface-to-bottom gradient is about 1.6‰ during the EOT.

The $\delta^{13}\text{C}$ values of benthic foraminifera in the CSV-1 core range from -0.9 to 1.3‰ (Fig. 9A and Supplementary Material 5). In the lower part of the NP21 zone, the carbon isotope values show a considerable decrease, followed by an increase from 422.8 to 406.8 m, then a significant decrease up to the top of the section. The $\delta^{13}\text{C}$ values of planktic foraminifera range from -1.3 to 0.9‰ and exhibit a similar trend to the carbon isotope curve of the benthic tests, without significant fluctuations. The planktic carbon isotope curve has a distinct peak at 412.1 m, from there the values decrease gradually upsection (Fig. 9A).

The $\delta^{13}\text{C}$ values of benthic foraminifera in the KL-1 core range from -0.4 to 1.2‰ , the record shows a gradual increase with brief positive excursions in the middle part of the section. From 88.5 m to the top of the section, the values decrease by 0.5 – 0.7‰ . A similar trend can be

observed in the $\delta^{13}\text{C}$ curve of planktic foraminifera, with slightly fluctuating values in the lower part of the section to 92.85 m, followed by a decrease of 0.5 – 0.7‰ upsection (Fig. 9B).

5. Discussion

5.1. Stable isotope records across EOT compared to global database

5.1.1. Oxygen isotope values

A fundamental question is whether our stable isotope geochemical data from the Paratethys show correlation with well-dated global isotopic and inferred paleoclimatic signals. It is well-established that a significant, 1.5‰ increase occurred in the global deep-sea $\delta^{18}\text{O}$ record during the EOT (e.g., Zachos et al., 2001; Coxall et al., 2005; Lear et al., 2008). This event was linked to the initial continental ice growth in the Southern Polar region (Miller et al., 1991; Coxall et al., 2005; Lear et al., 2008; Galeotti et al., 2016). Well-dated, high-resolution $\delta^{18}\text{O}$ and $\delta^{13}\text{C}$ isotope records derived from DSDP and ODP cores are available for the EOT (e.g., Zachos et al., 1994, 2001; Coxall et al., 2005; Katz et al., 2008; Miller et al., 2009). The compiled data and the fitted isotope curves are plotted in Fig. 10. Three major isotope events can be recognized: (1) EOT-1 (abbreviation for “Eocene-Oligocene transition event 1”), associated with an increase of 0.9‰ in $\delta^{18}\text{O}$, (2) EOT-2 (Eocene-Oligocene transition event 2), associated with a $\sim 0.8\text{‰}$ $\delta^{18}\text{O}$ increase (Miller et al., 2009), and (3) “Oi-1”, “Zone (Oligocene isotope 1)”, which was originally defined by Miller et al. (1991) and discussed later in detail by Coxall and Pearson (2007) and Pearson (2015) as an isotope zone of over three million years in duration. However, most workers use the term

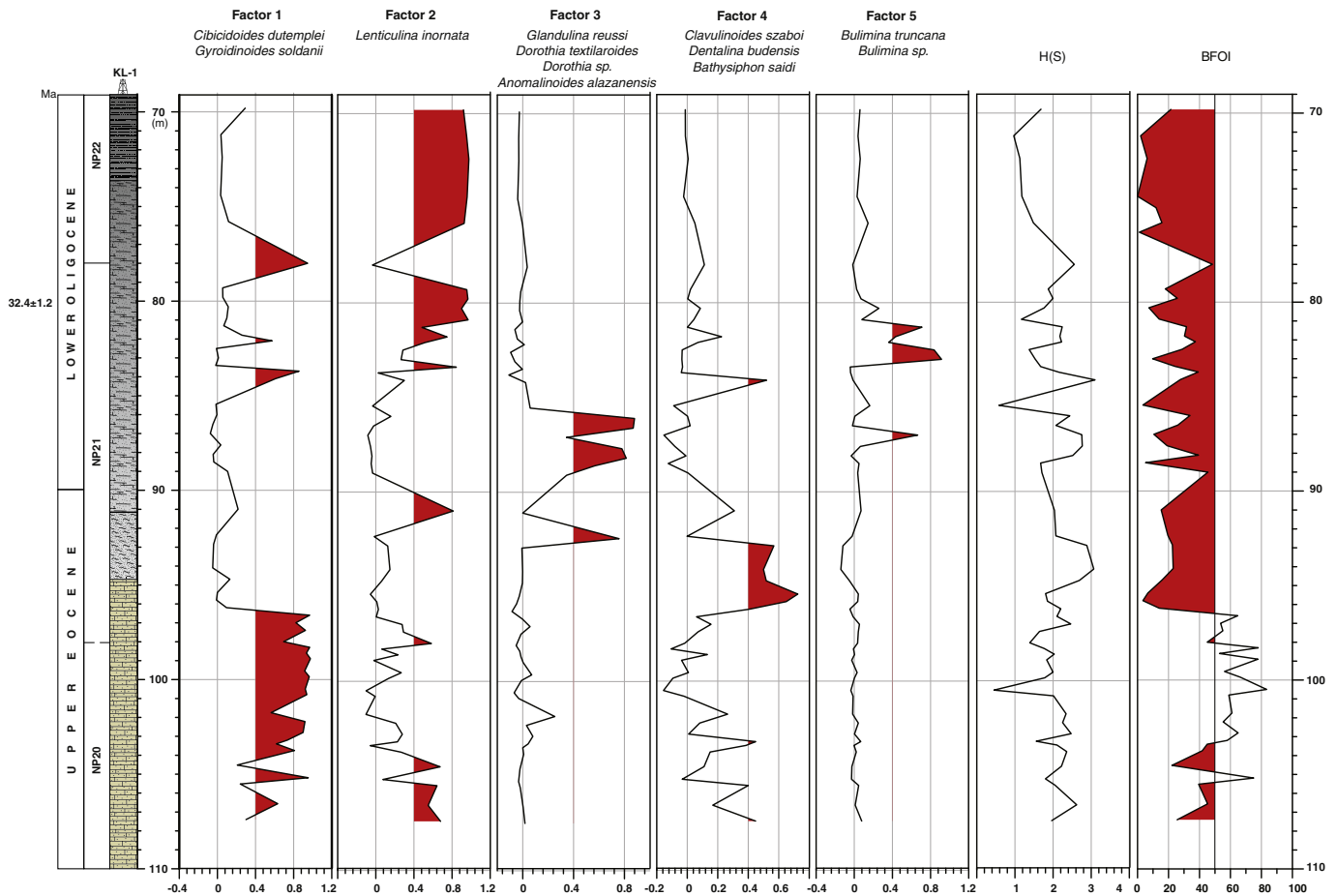


Fig. 7. Q-mode (Varimax-rotated) factor analysis, Diversity H(S) and benthic foraminiferal oxygen index (BFOI) vs. depth in the KL-1 borehole.

Oi-1 to denote the maximum positive $\delta^{18}\text{O}$ excursion during the early Oligocene, where $\delta^{18}\text{O}$ reaches maximum values at 33.55 Ma (Zachos et al., 1996; Katz et al., 2008; Miller et al., 2009) or at 33.65 Ma (Coxall and Wilson, 2011), in the records of DSDP Site 522 and ODP Sites 744 and 1218. This maximum value is associated to a significant sea-level fall (Miller et al., 2005). Our two $\delta^{18}\text{O}$ stable isotope curves show considerable similarity to the global curve throughout the investigated time interval, although the $\delta^{18}\text{O}$ values measured from the CSV-1 and KL-1 cores are systematically lower by 4 to 6‰ (Fig. 10). These very negative values would translate into unrealistically high seawater temperature during the EOT in the Paratethys, or they could imply that subsequent alteration affected the studied sections.

Trends in $\delta^{18}\text{O}$ values in the Oi-1 zone in the Paratethys mirror the global signal, although the magnitude of the ca. 2.5–3‰ increase is significantly higher than the $1.5 \pm 0.1\%$ shift in the global average record (Fig. 10). The similarity seems to be more obvious after standardizing the data from the CSV-1 borehole (Fig. 11) and, although the resolution of the global curve is much better, the isotope trends parallel the early Oligocene positive excursion. This suggests that the measured isotope values track the primary global signal with different amplitude.

The lower Oligocene record in the Paratethys shows elevated $\delta^{18}\text{O}$ above the E-O boundary, as is typical of the global deep ocean (Fig. 10). These records provide the first evidence of globally synchronous change in $\delta^{18}\text{O}$ representing EOT climatic change in the bathyal environment of the Paratethys, although direct estimates for the paleotemperature cannot be made. The results of the Q-mode factor analysis show that epifaunal *C. dutemplei* and associated forms (Factor

1, see Fig. 6) dominated around the EOT time in both investigated sections. This dominantly oligotrophic to mesotrophic fauna is a characteristic constituent of modern shelf and upper bathyal regions (e.g., Jorissen, 1987; Schiebel, 1992; Murray, 2006), where the effect of sea surface temperature (e.g., seasonal fluctuations) is negligible. Therefore we conclude that the detected increase in benthic $\delta^{18}\text{O}$ might have been triggered when isotopically heavy and/or cool bottom-water appeared in different subbasins of the Paratethys. Following the maximum excursion of benthic $\delta^{18}\text{O}$ (above 405 m in CSV-1 and around 92 m in KL-1 borehole), a significant decrease (1.5–3‰) can be detected in the Paratethys, compared to 0.5–1‰ in the global average (Fig. 10). This more pronounced rebound in the Paratethys might record the progress of its first isolation from the surrounding open ocean (Báldi, 1984).

Significantly fewer studies have concentrated on the stable isotope composition of planktic foraminifera during the EOT, because the $\delta^{18}\text{O}$ composition of their tests is strongly influenced by regional water mass salinity changes. Planktic foraminifera live in a wide range of depth in the upper part of ocean column (0–500 m), where the temperature varies from ~30 °C to 8 °C (Birch et al., 2013). The very high standard deviation of planktic foraminiferal $\delta^{18}\text{O}$ signals in the global data set hints at a conspicuous north-south, near-surface oceanic temperature gradient during the EOT. In addition, any local environmental change such as seasonal fluctuations, enhanced river run-off and freshwater input might cause strong fluctuations in the planktic $\delta^{18}\text{O}$ values. Planktic $\delta^{18}\text{O}$ data range from –3.8‰ to 3‰ in the global database, compared to –6‰ to –3‰ in the Paratethys. Again, the apparently anomalous low isotope values would allow inference of unrealistically

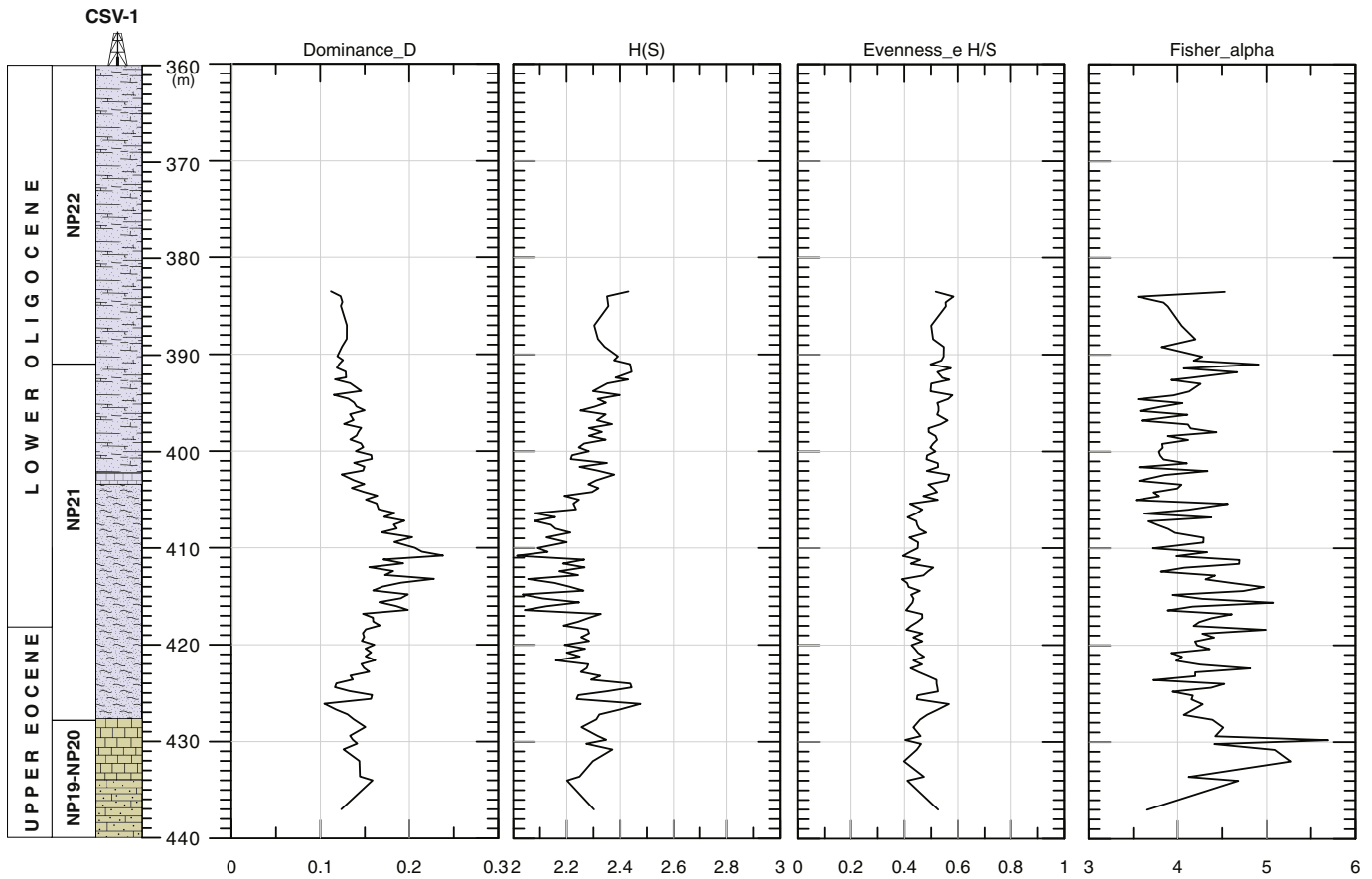


Fig. 8. Calcareous nannoplankton dominance (Dominance_D), diversity (H(S)), evenness (Evenness_e H/S) and Fisher alpha index vs. depth in the CSV-1 borehole.

high SST for the Paratethys or, alternatively, the development of reduced-salinity surface water mass. Comparably low oxygen isotopic values were documented in sapropels deposited during a seasonal low-salinity interval in the eastern Mediterranean during the past 13,000 years (Tang and Stott, 1993). This condition extended throughout the fall and winter periods and it was most probably triggered by significant freshwater input into the basin, possibly associated with a pluvial period. Similar paleoceanographic conditions are assumed for the Slovenian Paleogene Basin (Fig. 1) during the Oligocene (Schmiedl et al., 2003) and for the Inneralpine Molasse Basin (Fig. 2) during the late Oligocene (Scherbacher et al., 2001). In addition, the significant input of lower density freshwater probably caused stratification in the water column, which led to temporarily anoxic conditions in the deeper subbasins of Central Paratethys, and the formation of brackish conditions in the shallower, near-coastal areas within two million years. By comparing the planktic and benthic $\delta^{18}\text{O}$ values, covariant offset can be observed in the $\delta^{18}\text{O}$ signals. The planktic $\delta^{18}\text{O}$ values are systematically lighter than their benthic counterparts in all samples (Fig. 9). The average observed surface-to-bottom gradient was about 1.6‰ during the EOT, indicating at least partial preservation of the expected ecological offset.

5.1.2. Carbon isotope values

The $\delta^{13}\text{C}$ value of biogenic carbonate in foraminiferal test is primarily controlled by the $\delta^{13}\text{C}$ value of ambient dissolved inorganic carbon (Mook, 1968). The global carbon curve shows a $>1\%$ $\delta^{13}\text{C}$ increase (Fig. 10) during the EOT which is traceable in our $\delta^{13}\text{C}$ curves (Fig. 10), although the values are ca. 1‰ lighter in the Paratethys than the global average. Various hypotheses have been put forward to explain the increase in global $\delta^{13}\text{C}$ values during this period. One of

them proposes that increased organic nutrient flux into oceanic basins caused increased C_{org} burial (e.g., Salamy and Zachos, 1999; Dunkley Jones et al., 2008; Coxall and Wilson, 2011). The second model (Merico et al., 2008) suggests enhanced inorganic input into oceanic basins by weathering of shelf carbonates associated to EOT-related sea-level fall (e.g., Miller et al., 2005). The positive $\delta^{13}\text{C}$ anomaly and the appearance of infaunal or shallow infaunal benthic foraminifera such as *Uvigerina* (Factor 2) and *Bathysiphon* (Factor 4) and associated species in the CSV-1 core (Fig. 6), and *Clavulinoides* (Factor 4), *Glandulina* (Factor 3) and *Lenticulina* (Factor 2) and associated species in the KL-1 core suggest that high organic carbon flux characterizes the Hungarian Paleogene Basin from the middle part of NP21 nannozone (at 405 m in CSV-1 and around 92 m in KL-1 borehole). These infaunal or shallow infaunal benthic foraminifera are most abundant in the upper 5 cm of organic-rich sediments in modern outer shelf and bathyal regions (e.g., Gooday et al., 2002; Fontanier et al., 2002; Murray, 2006). These forms usually occur in high productivity areas along with the oxygen minimum zone in deeper basins, as a number of studies documented them from similar environments, e.g., in the lower Oligocene of the Inneralpine Molasse Basin (Scherbacher et al., 2001) or in the upper Paleogene of the Slovenian Paleogene Basin (Schmiedl et al., 2002). The dominance of infaunal and shallow infaunal benthic foraminiferal species (inferred from significant loadings of the FC-2 to FC-5 between 415 m and 370 m in the CSV-1 borehole and 95 m to 70 m in KL-1 borehole) is thought to represent a decrease in oxygen concentration of bottom water over the Eocene-Oligocene boundary. Simultaneously, BFOI values show a gradual decrease in the CSV-1 borehole from 405 m and generally low values from 92 m in the KL-1 borehole (Figs. 6, 7, and 10), confirming the onset of eutrophic and oxygen-limited conditions in the Paratethyan area (Fig. 2). Above the Eocene/Oligocene

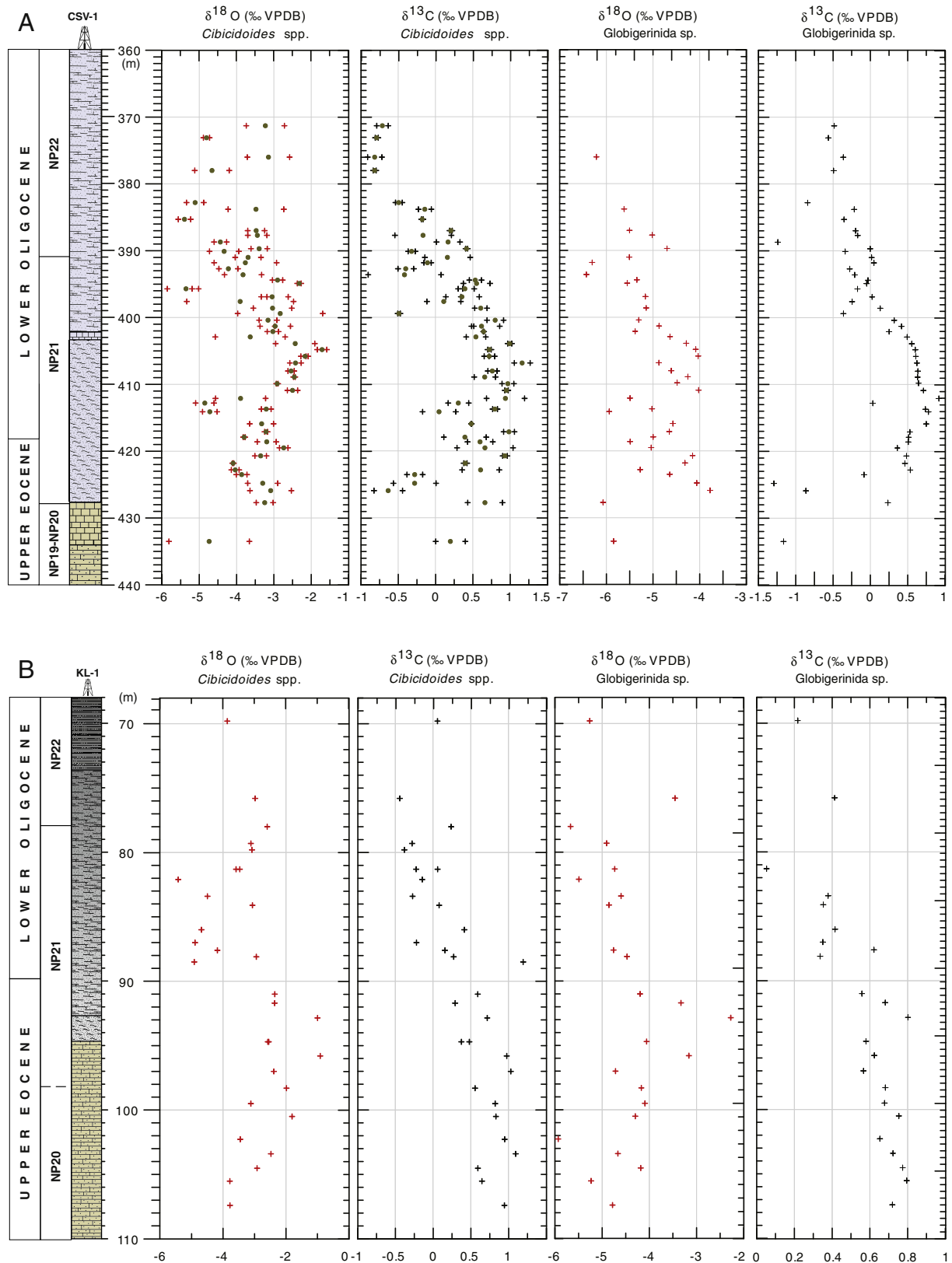


Fig. 9. A. Benthic foraminifera (*Cibicides* spp.) and planktic foraminifera (*Globigerina* sp.) oxygen and carbon isotope (per-mil VPDB) time series from the CSV-1 borehole plotted vs. age for the EOT. Age model based on nannoplankton stratigraphy (Berggren et al., 2012). B. Benthic foraminifera (*Cibicides* spp.) and planktic foraminifera (*Globigerina* sp.) oxygen and carbon isotope (per-mil VPDB) time series from the KL-1 borehole plotted vs. age for the EOT. Age model based on nannoplankton stratigraphy (Berggren et al., 2012).

boundary the $\delta^{13}\text{C}$ values show an overall similar pattern to the global carbon curve, except for a more significant decrease above the EOT (Fig. 10), where 1.0–1.2‰ lighter $\delta^{13}\text{C}$ values are recorded. This

confirms that carbon isotopic evolution of the Paratethys follows the global signal until the end of EOT, whereas the subsequent departure from the global signal is consistent with the hypothesis that the

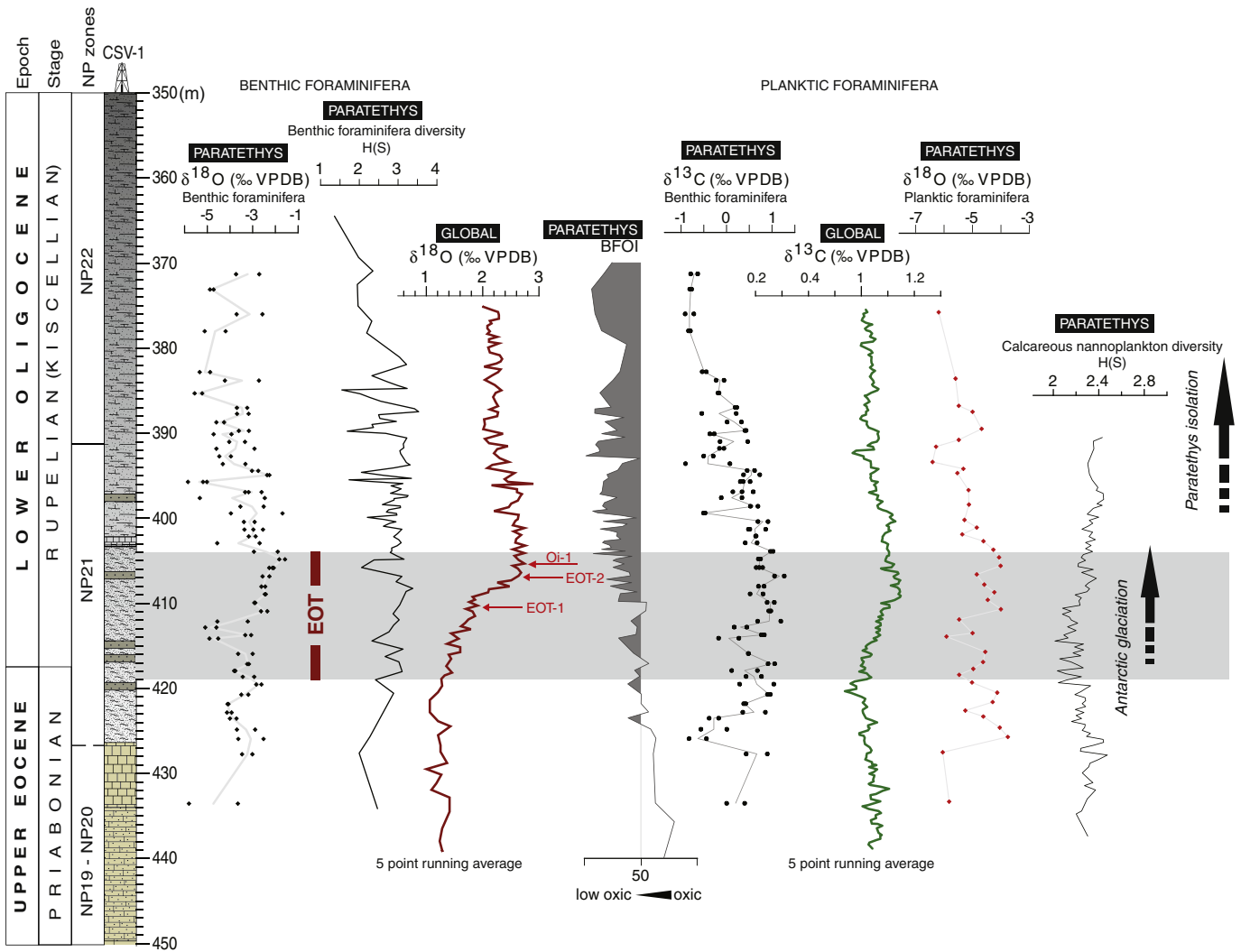


Fig. 10. Oxygen isotope curves of benthic foraminifera from the CSV-1 and KL-1 boreholes and a composite global deep-sea oxygen isotope curve. Raw data for the global curve are based on benthic foraminifera from DSDP 77, DSDP 522, DSDP 529, DSDP 563, DSDP 574, ODP 689, ODP 744, ODP 748 and ODP 1218 sites (after Grossman, 2012). The average curve was smoothed using a 5-point running mean of data listed in Supplementary material 5. The shaded region represents the EOT, where the greenhouse-to-icehouse transition culminated in the earliest Oligocene.

Paratethys became isolated from the surrounding open oceans after the Antarctic glaciation event and associated climatic cooling.

5.2. Primary signal vs. diagenetic overprint

Our stable isotope analyses of benthic and planktic foraminifera yielded $\delta^{18}\text{O}$ values that are systematically lower than the global oxygen isotope data from the same interval (Fig. 10). The unexpectedly negative $\delta^{18}\text{O}$ values may indicate subsequent alteration that affected the foraminifer tests, and/or increased precipitation (e.g., monsoon effect) during the EOT in the Paratethyan area.

5.2.1. Diagenesis

Low $\delta^{18}\text{O}$ values may imply diagenetic overprint that would hinder paleoenvironmental interpretation. SEM observations suggest that the shell structure is well-preserved and recrystallization was negligible (Fig. 5A and B), thus it could not account for a significant offset from the primary isotope values. This is further supported by the black CL pattern of the shell, indicating oxidative conditions during precipitation. In contrast, the chamber-filling calcite displays uniform, bright orange CL color (Fig. 5D) and implies precipitation from slightly reducing fluids.

The unexpectedly low $\delta^{18}\text{O}$ values are probably due to the calcite cement in the tests, which may have precipitated from either the pore fluids of elevated temperature during deep burial, or hydrothermal and/or meteoric fluids circulating through the pore space during uplift.

Deep burial diagenetic cement precipitating from marine pore fluids of elevated temperature at greater depth would have depleted oxygen isotopic composition, proportional to the depth. However, it is unlikely that the tests remained unfilled at burial depth in excess of 1000 m. The bright CL of the calcite suggests only slightly reducing parent fluid that is in contrast to what is expected at such depth.

The other scenario invokes precipitation of calcite cement from fluids with low $\delta^{18}\text{O}$ values during uplift which started in the Miocene. Such fluids may have been sourced from hydrothermal fluids in the Paleogene basin (Poros et al., 2012). However, this process would require that the chambers of foraminifera remained unfilled for at least 20 Myr. Empty foraminifera tests were reported at ca. 400 m depth both from Eocene microporous limestone (Maliva et al., 2009) and Cretaceous chalk (Price et al., 1998). Although the lithology and diagenetic history of these rocks differ significantly from the those studied here, the possibility remains (and its testing awaits further study) that the tests stayed open until calcite precipitated in the chambers from fluids with low $\delta^{18}\text{O}$ values at elevated temperature, either during deep burial or subsequent uplift.

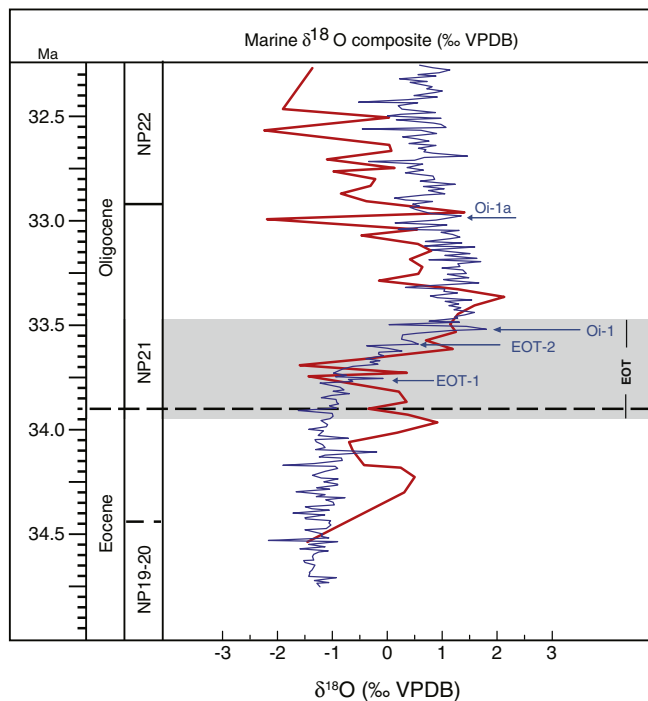


Fig. 11. Comparison of the composite global deep-sea oxygen isotope curve (blue) and the standardized oxygen isotope values from the CSV-1 borehole (red). Calculation of standard scores (z) follows the equation $z_i = (x_i - x_m)/\sigma$, where x_m is the mean and σ is the standard deviation of the measured isotope values. (For interpretation of the references to in this figure legend, the reader is referred to the web version of this article.)

5.2.2. Increased precipitation (monsoon effect)

Increased freshwater input into the basin may represent another possible cause of deviation in $\delta^{18}\text{O}$ values. In the modern Indian Ocean and eastern Mediterranean Sea, intense monsoon precipitation delivers large amounts of isotopically light freshwater through discharge of the Padma and Nile Rivers, respectively (Rossignol-Strick et al., 1982), recorded in low $\delta^{18}\text{O}$ values of planktic foraminifera (Tang and Stott, 1993). By analogy, development of a surficial freshwater lens might have reduced the exchange between surface and deeper waters, leading to water column stratification and temporarily anoxic conditions in the deeper subbasins of the Central Paratethys (Schmiedl et al., 2002). Development of low-salinity surface water masses in the Central Paratethys is indicated by the appearance of mono- and duospecific calcareous nannoplankton assemblages from the late early Oligocene (NP23), leading to the disappearance of benthic communities within two million years. Stable isotopic composition of the tooth enamel of late Paleogene large terrestrial mammals from Europe reflects a significant increase in rainfall, especially from the NP23 zone (Kocsis et al., 2014). Paleobotanical analyses also suggest high humidity during the EOT in the terrestrial environment around the Hungarian Paleogene Basin (Erdei et al., 2012).

6. Paleoclimatic and paleoceanographic changes in the Hungarian Paleogene Basin during the Eocene-Oligocene climate transition

The largest global paleoclimatic event in the Cenozoic is closely associated with the establishment of the Antarctic ice cap (Shackleton and Kennett, 1975; Zachos et al., 1996, 2001; Salamy and Zachos, 1999; Coxall et al., 2005; Pearson et al., 2009; Galeotti et al., 2016), and it is expected to have influenced the regional climate regime in the Central Paratethys area. Our micropaleontological record suggests significant changes during the EOT in both the bottom and surface waters (Fig. 10). Benthic foraminiferal communities indicate dominantly

oligotrophic to mesotrophic environment at the end of the late Eocene (Priabonian) and the earliest Oligocene (early Rupelian) (Fig. 12A). From the middle early Oligocene, eutrophication resulted in increasing flux of organic matter to the sea floor (Fig. 12B). However, temporarily anoxic conditions did not develop before the late early Oligocene, when the dissolved oxygen content dropped below 1.5 ml/l. The positive $\delta^{13}\text{C}$ anomaly and the appearance of infaunal and shallow infaunal benthic foraminiferal species over the Eocene-Oligocene boundary (where the BFOI shows gradual decrease in the investigated sections) also confirm the onset of eutrophic and oxygen-limited conditions in the Paratethys (Figs. 10 and 12C). This event coincides with increasing $\delta^{18}\text{O}$ values of benthic foraminifera, which reflects the development of continental ice sheet in Antarctica. The decrease of benthic foraminiferal diversity in the late early Oligocene with very low values of BFOI is congruent with these changes (Figs. 10 and 12D) and the isolation of Paratethys from the western Tethys Ocean after the EOT, as suggested by Báldi (1984).

The presence of marine, tropical to subtropical nannoplankton associations in the late Eocene suggests a marine connection (Fig. 12A) to the surrounding open ocean of the Indopacific realm. The appearance of nearshore nannoplankton groups indicates that this marine connection became limited towards the Western Tethys during the EOT. The decrease in nannoplankton diversity and highest dominance of *Helicosphaera* indicate strong variability of salinity and enhanced terrestrial fluxes (Fig. 12B). Our stable isotope records show a significant decrease later, after the EOT (Fig. 10), which differs from the global trend, and it is probably related to the isolation of Paratethys from the Western Tethys and the Atlantic Ocean. The initial isolation process might have coincided with a second-order sea-level fall and the orogenic uplift of the Alpine-Carpathian-Dinaride chain (Fig. 12B–D). Subsequently, a major increase in freshwater input probably caused stratification of the water column, which led to the formation of temporarily anoxic bottom-waters in the deeper subbasins of the Central Paratethys, and the development of brackish conditions in the shallower, near-coastal areas within two million years, by the late early Oligocene.

7. Conclusions

New micropaleontological and stable isotope data from the Central Paratethys provide insight into the paleoclimatological, paleoceanographical and paleoenvironmental evolution in this epicontinental sea during the Eocene-Oligocene climate transition. The benthic foraminiferal faunas of both studied Eocene-Oligocene borehole sections in the Hungarian Paleogene Basin suggest relatively stable paleobathymetry from the late Eocene to early Oligocene. Benthic communities are characterized by epifaunal genera during the late Eocene and by shallow to deep infaunal genera during the early Oligocene. Benthic foraminiferal diversity is slightly increasing across the EOT, while a significant decrease can be observed in the late early Oligocene.

The calculated BFOI values suggest higher than 3 ml/l O_2 concentration at both sites during the late Eocene and a decrease across the EOT, indicating low oxic depositional environment. The estimated O_2 concentration in bottom-water ranges between 1.5 and 3.0 ml/l. The BFOI shows the lowest values after the EOT across the whole investigated time interval, indicating approximately 0.3 to 1.5 ml/l dissolved oxygen content. Based on multivariate statistical analyses of the nannoplankton flora, two ecological groups can be distinguished: a pelagic, normal-salinity nannoplankton association in the late Eocene, which indicates fully open marine connections, and a nearshore nannoplankton association during and after the EOT, with taxa which prefer cooler climate and are able to tolerate varying salinity and increase in terrestrial influx.

The stable isotope analyses of benthic and planktic foraminifera from the Paratethys reveal that the measured $\delta^{18}\text{O}$ and $\delta^{13}\text{C}$ values display the same trends but are systematically lower relative to global

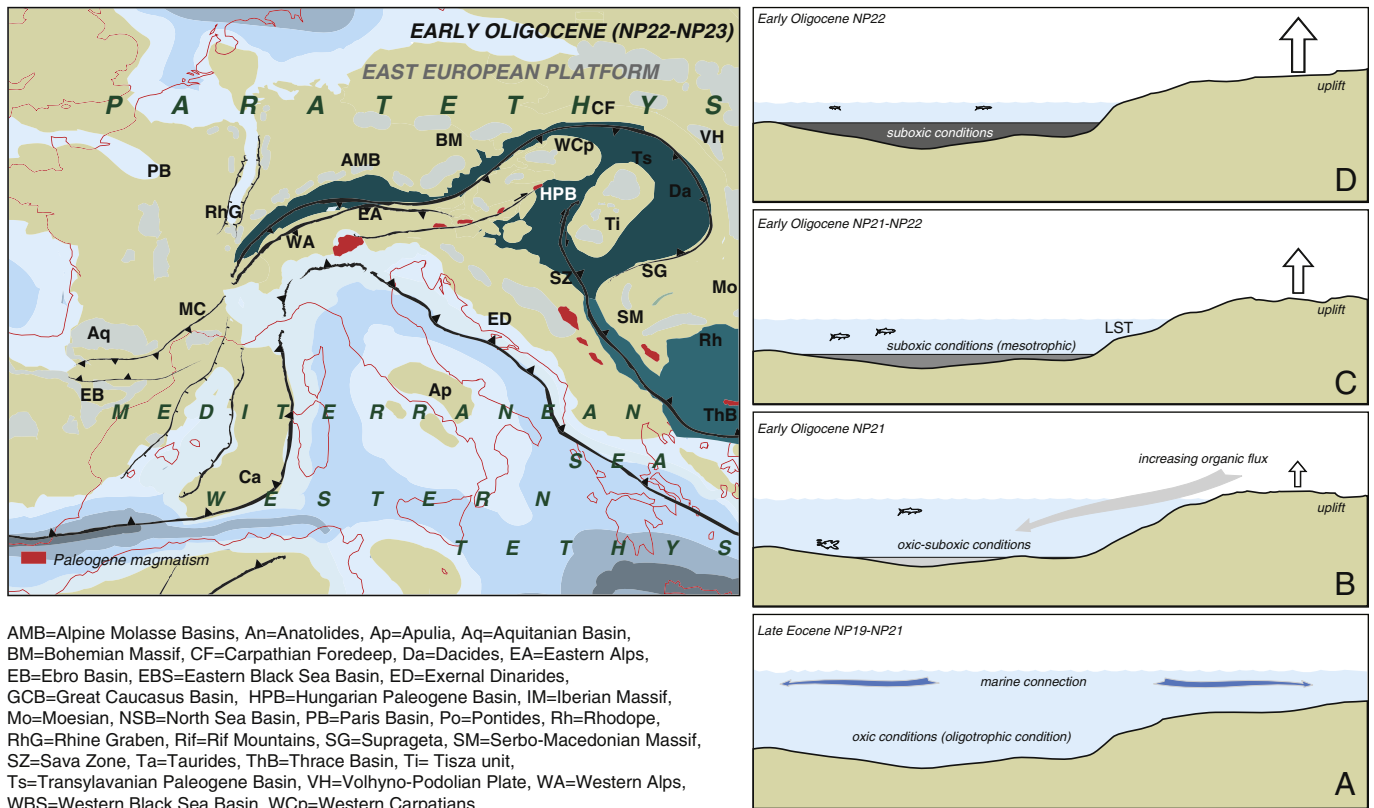


Fig. 12. Paleogeographic reconstruction and paleoceanographic model for the HPB (Paratethys) during the EOT (NP22-NP23 zones). Paleogeographic map illustrate the isolation of Paratethys from the surrounding open oceans after the EOT. The presented paleogeographic reconstruction is based on paleogeographic maps of Ziegler (1990), Dercourt et al. (1993), Rögl (1998), Meulenkamp and Sissingh (2003) and Popov et al. (2004). Paleogeographic models: A. Oligotrophic to mesotrophic environment at the end of the late Eocene and earliest part of the early Oligocene with marine connections to the surrounding open ocean. B. Increasing flux of organic matter to the sea floor resulted in eutrophication from the middle early Oligocene. C. The initial isolation process might have coincided with a second-order sea-level drop (manifest in a lowstand systems tract) and the orogenic uplift of the Alpine-Carpathian-Dinaride chain. D. Freshwater input probably caused stratification of the water column, which led to the formation of suboxic conditions in the Central Paratethys.

oxygen isotope data compiled for the investigated period. The positive $\delta^{18}\text{O}$ shift at the EOT in the Paratethys coincides with the global trends in the signal, and it reflects the influence of this global climatic event in the Paratethys. The planktic $\delta^{18}\text{O}$ values are systematically lower than their benthic counterparts, indicating at least partial preservation of expected ecological offset, thus providing further evidence that the stable isotope signals reported here are not completely masked by diagenetic alteration.

The positive $\delta^{13}\text{C}$ anomaly and the synchronous appearance of infaunal or shallow infaunal benthic foraminifera suggest that increasingly high organic carbon flux and burial rate characterized the Hungarian Paleogene Basin from the Eocene-Oligocene boundary.

The $\delta^{18}\text{O}$ and $\delta^{13}\text{C}$ values show an overall similar pattern to the compiled global isotope curves during the EOT, although a more significant decrease can be observed after this global event. This deviation suggests that the Paratethys became completely isolated from the surrounding open oceans after the EOT.

Supplementary data to this article can be found online at <http://dx.doi.org/10.1016/j.palaeo.2016.07.034>.

Acknowledgments

The authors are thankful to János Csizmeg, János Haas, Attila Petrik, István Vető and Helmut Weissert for discussions on diagenesis. This research was supported in part by a Bolyai Research Scholarship to PO (BO/00694/08/10) and by the Hungarian Science Foundation (OTKA) project K112708. LK was supported by the Swiss National Science Foundation (SNF PZ00P2_126407) during this work. We are very grateful to Helen Coxall and an anonymous reviewer for their very constructive reviews. The helpful comments of journal editor Thomas Algeo through all

stages handling the manuscript were greatly appreciated. This is MTA-MTM-ELTE Paleo Contribution No. 219.

References

- Báldi, T., 1984. The terminal Eocene and Early Oligocene events in Hungary and the separation of an anoxic, cold Paratethys. *Eclogae Geol. Helv.* 77, 1–27.
- Báldi, T., 1986. Mid-Tertiary Stratigraphy and Paleogeographic Evolution of Hungary. *Akadémiai Kiadó, Budapest*.
- Báldi, T., Báldi-Beke, M., 1985. The evolution of the Hungarian Paleogene Basin. *Acta Geol. Hung.* 28, 5–28.
- Báldi, T., Horváth, M., Nagymarosy, A., Varga, P., 1984. The Eocene-Oligocene boundary in Hungary. *The Kiscellian stage. Acta Geol. Hung.* 27, 41–65.
- Báldi-Beke, M., 1972. The nannoplankton of the Upper Eocene bryozoa and Buda Marls. *Acta Geol. Hung.* 16, 211–228.
- Báldi-Beke, M., 1977. Stratigraphical and faciological subdivision of the Oligocene as based on nannoplankton. *Földtani Közlemény* 107, 59–89.
- Báldi-Beke, M., 1984. The nannoplankton of the Transdanubian Paleogene formations. *Geol. Hung. Ser. Palaeontol.* 43, 1–307.
- Báldi-Beke, M., Báldi, T., 1991. Palaeobathymetry and palaeogeography of the Bakony Eocene Basin in western Hungary. *Palaeogeogr. Palaeoclimatol. Palaeoecol.* 88, 25–52.
- Bechtel, A., Hámor-Vidó, M., Gratz, R., Sachsenhofer, R.F., Püttmann, W., 2012. Facies evolution and stratigraphic correlation in the early Oligocene Tard clay of Hungary as revealed by maceral, biomarker and stable isotope composition. *Mar. Pet. Geol.* 35, 55–74.
- Berggren, W.A., Alegret, L., Aubry, M.-P., Cramer, B.S., Dupuis, C., Goolaeert, S., Kent, D.V., King, C., Knox, R.W.O., Obaidalla, N., Ortiz, S., Ouda, K.A.K., Abdel-Sabour, A., Salem, R., Senosy, M.M., Soliman, M.F., Soliman, A., 2012. The Dababya corehole, Upper Nile Valley, Egypt: preliminary results. *Austrian J. Earth Sci.* 105, 161–168.
- Birch, H., Coxall, H.K., Pearson, P.N., Kroon, D., O'Regan, M., 2013. Planktonic foraminifera stable isotopes and water column structure: disentangling ecological signals. *Mar. Micropaleontol.* 10, 127–145.
- Blow, W.H., 1969. Late middle Eocene to Recent planktonic foraminiferal biostratigraphy. In: Bronnimann, P., Renz, H.H. (Eds.), *Proceedings of the First International Conference on Planktonic Microfossils*, pp. 199–421.
- Bown, P.R., 1998. Calcareous nannofossil biostratigraphy. *Nannoplankton Res.* 19, 36–47.
- Bukry, D., 1974. Coccoliths as paleosalinity indicators - evidence from Black Sea. In: Degens, E.T., Ross, D.D. (Eds.), *The Black Sea—Geology, Chemistry and*

- Biology American Association of Petroleum Geologists Memoir 20. American Association of Petroleum Geologists, Tulsa, OK, pp. 353–363.
- Buzas, M.A., Gibson, T.G., 1969. Species diversity: benthonic foraminifera in the western North Atlantic. *Science* 163, 72–75.
- Corliss, B.H., 1991. Morphology and microhabitat preferences of benthic foraminifera from the northwest Atlantic Ocean. *Mar. Micropaleontol.* 17, 195–236.
- Coxall, H.K., Pearson, P.N., 2007. The Eocene–Oligocene transition. In: Williams, M., Haywood, A.M., Gregory, F.J., Schmidt, D.N. (Eds.), *Deep-Time Perspectives on Climate Change: Marrying the Signal from Computer Models and Biological Proxies*. Geological Society, Micropaleontological Society, London, pp. 351–387.
- Coxall, H.K., Wilson, P.A., 2011. Early Oligocene glaciation and productivity in the eastern equatorial Pacific: insights into global carbon cycling. *Paleoceanography* 26, PA2221.
- Coxall, H.K., Wilson, P.A., Pälike, H., Lear, C.H., Backaman, J., 2005. Rapid stepwise of Antarctic glaciation and deeper calcite compensation in the Pacific Ocean. *Nature* 433, 53–57.
- Csontos, L., Nagymarosy, A., Horváth, F., Kovács, M., 1992. Tertiary evolution of the intra-Carpathian area: a model. *Tectonophysics* 208, 221–241.
- DeConto, R.M., Pollard, D., Harwood, D., 2007. Sea ice feedback and Cenozoic evolution of Antarctic climate and ice sheet. *Paleoceanography* 22, PA3214.
- Dercourt, J., Ricou, L.E., Vrielynck, B., 1993. Atlas Tethys palaeoenvironmental maps. 14 maps. Gauthier-Villars, Paris (307 pp.).
- Dunkley Jones, T., Bown, P.R., Pearson, P.N., Wade, B.S., Coxall, H.K., Lear, C.H., 2008. Major shifts in calcareous phytoplankton assemblages through the Eocene–Oligocene transition of Tanzania and their implications for low-latitude primary production. *Paleoceanography* 23, PA4204.
- Erdei, B., Utescher, T., Hably, L., Tamás, J., Roth-Nebelsick, A., Grein, M., 2012. Early Oligocene continental climate of the Palaeogene Basin (Hungary and Slovenia) and the surrounding area. *Turk. J. Earth Sci.* 21, 153–186.
- Fontanier, C., Jorissen, F.J., Licari, L., Alexandre, A., Anschutz, P., Carbonel, P., 2002. Live benthic foraminiferal faunas from the Bay of Biscay: faunal density, composition, and microhabitats. *Deep-Sea Res.* 149, 751–785.
- Galeotti, S., DeConto, R., Naish, T., Stocchi, P., Florindo, F., Pagani, M., Barrett, P., Bohaty, S.M., Lanci, L., Pollard, D., Sandroni, S., Talarico, F.M., Zachos, J.C., 2016. Antarctic ice sheet variability across the Eocene–Oligocene boundary climate transition. *Science* 352, 76–80.
- Gooday, A.J., Pond, D.W., Bowser, S.S., 2002. Ecology and nutrition of the large agglutinated foraminiferan *Bathysiphon capillare* in the bathyal NE Atlantic: distribution within the sediment profile and lipid biomarker composition. *Mar. Ecol. Prog. Ser.* 245, 69–82.
- Grossman, E., 2012. Oxygen isotope stratigraphy. In: Gradstein, F., Ogg, J. (Eds.), *The Geological Time Scale 2012*. Elsevier (chapter 10).
- Hammer, O., Harper, D.A.T., Ryan, P.D., 2001. PAST: paleontological statistics software package for education and data analysis. *Paleoentol. Electron.* 4 (1) (9 pp., http://paleo-electronica.org/2001.1/past/issue1_01.htm).
- Horváth, F., Bada, G., Windhoffer, G., Csontos, L., Dövényi, P., Fodor, L., Grenerczy, G., Síkhegyi, F., Szafián, P., Székely, B., Timár, G., Tóth, L., Tóth, T., 2005. Atlas of the present-day geodynamics of the Pannonian basin: Euroconform maps with explanatory text. http://geophysics.elte.hu/atlas/geodin_atlas.htm.
- Jorissen, F.J., 1987. The distribution of benthic foraminifera in the Adriatic Sea. *Mar. Micropaleontol.* 12, 21–49.
- Jorissen, F.J., De Stigter, H.C., Widmark, J.G.V., 1995. A conceptual model explaining benthic foraminiferal microhabitats. *Mar. Micropaleontol.* 22, 3–15.
- Kaiho, K., 1994. Benthic foraminiferal dissolved-oxygen index and dissolved-oxygen levels in the modern ocean. *Geology* 22, 719–722.
- Katz, M.E., Miller, K.G., Wright, J.D., Wade, B.S., Browning, J.V., Cramer, B.S., Rosenthal, Y., 2008. Stepwise transition from the Eocene greenhouse to the Oligocene icehouse. *Nat. Geosci.* 1, 329–334.
- Kázmér, M., 1985. Sedimentological investigation of the Eocene–Oligocene boundary sequence in the Kiscell-1 borehole. *Őslénytani Viták* 31, 71–74.
- Kázmér, M., Dunkl, I., Frisch, W., Kuhlemann, J., Ozsvárt, P., 2003. The Palaeogene forearc basin of the Eastern Alps and Western Carpathians: subduction erosion and basin evolution. *J. Geol. Soc.* 160, 413–428.
- Kocsis, L., Ozsvárt, P., Becker, D., Ziegler, R., Scherler, L., Codrea, V., 2014. Orogeny forced terrestrial climate variation during the late Eocene–early Oligocene in Europe. *Geology* 42, 727–730.
- Lear, C.H., Bailey, T.R., Pearson, P.N., Coxall, H.K., Rosenthal, Y., 2008. Cooling and ice growth across the Eocene–Oligocene transition. *Geology* 36, 251–254.
- Mackensen, A., Sejrup, H.P., Jansen, E., 1985. The distribution of living benthic foraminifera on the continental slope and rise off southwest Norway. *Mar. Micropaleontol.* 9, 275–306.
- Maliwa, R.G., Missimer, T.M., Clayton, E.A., Dickson, J.A.D., 2009. Diagenesis and porosity preservation in Eocene microporous limestones, South Florida, USA. *Sediment. Geol.* 217, 85–94.
- Maravelis, A., Zeligidis, A., 2012. Paleoclimatology and paleoecology across the Eocene/Oligocene boundary, Thrace basin, Northeast Aegean Sea, Greece. *Paleoogeogr. Palaeoclimatol. Palaeoecol.* 365–366, 81–98.
- Martini, E., 1970. Standard Paleogene calcareous nannoplankton zonation. *Nature* 226, 560–561.
- Martini, E., 1971. Standard tertiary and quaternary calcareous nannoplankton zonation. *Proceedings of the II Planktonic Conference, Roma 1970*, pp. 739–785.
- Merico, A., Tyrrell, T., Wilson, P.A., 2008. Eocene/Oligocene Ocean de-acidification linked to Antarctic glaciation by sea-level fall. *Nature* 452, 979–982.
- Meulenkamp, J.E., Sissingh, W., 2003. Tertiary palaeogeography and tectonostratigraphic evolution of the northern and southern Peri-Tethys platform and the intermediate domains of the African–Eurasian convergent plate boundary zone. *Paleoogeogr. Palaeoclimatol. Palaeoecol.* 196, 206–228.
- Miller, K.G., Wright, J.D., Fairbanks, R.G., 1991. Unlocking the Ice House: Oligocene–Miocene oxygen isotopes, eustasy and margin erosion. *J. Geophys. Res.* 96, 6829–6848.
- Miller, K.G., Komazin, M.A., Browning, J.V., Wright, J.D., Mountain, G.S., Katz, M.E., Sugarman, P.J., Cramer, B.S., Christie-Blick, N., Pekar, S.F., 2005. The Phanerozoic record of global sea-level change. *Science* 310, 1293–1298.
- Miller, K.G., Wright, J.D., Katz, M.E., Wade, B.S., Browning, J.V., Cramer, B.S., Rosenthal, Y., 2009. Climate threshold at the Eocene–Oligocene transition: Antarctic ice sheet influence on ocean circulation. *Geol. Soc. Am. Spec. Pap.* 452, 169–178.
- Mook, W., 1968. *Geochemistry of the Stable Carbon and Oxygen Isotopes of Natural Waters in the Netherlands*. University of Groningen, Groningen, Netherlands.
- Murray, J.W., 2006. *Ecology and Applications of Benthic Foraminifera*. Cambridge University Press.
- Nagymarosy, A., 1985. Calcareous nannoplankton of the lower Oligocene and Eocene–Oligocene transition units in Hungary. *Őslénytani Viták* 31, 25–28.
- Nagymarosy, A., Báldi-Beke, M., 1988. The position of the Paleogene formations of Hungary in the standard nannoplankton zonation. *Annales Universitatis Scientiarum Budapestinensis de Rolando Eötvös Nominatae Sectio Geologica* 28, pp. 3–25.
- Nyerges, A., 2014. *A Cserépváralja-1 Fúrás Felső Eocén–alsó Oligocén Nannoplankton Flórájának Kvantitatív Elemzése és Biosztratifrágiái Feldolgozása* (MSc Thesis) Eötvös Loránd Egyetem, Budapest, p. 67.
- Ozsvárt, P., 2007. Middle and Late Eocene benthic foraminiferal fauna from the Hungarian Paleogene Basin: systematics and paleoecology. *Geol. Pannonica Spec. Pap.* 2, 1–129.
- Pagani, M., Zachos, J.C., Freeman, K.H., Tipple, B., Bohaty, S., 2005. Marked decline in atmospheric carbon dioxide concentrations during the Paleogene. *Science* 309, 600–603.
- Pearson, P.N., 2015. Interactive comment on “The Eocene–Oligocene transition at ODP Site 1263, Atlantic Ocean: decreases in nannoplankton size and abundance and correlation with benthic foraminiferal assemblages” by M. Bordiga et al. *Clim. Past Discuss.* 11, C838–C841.
- Pearson, P.N., Foster, G.L., Wade, B.S., 2009. Atmospheric carbon dioxide through the Eocene–Oligocene climate transition. *Nature* 461, 1110–1114.
- Perch-Nielsen, K., 1985. *Cenozoic calcareous nannofossils*. In: Bolli, H.M., Saunders, J.B., Perch-Nielsen, K. (Eds.), *Plankton Stratigraphy*. Cambridge University Press, Cambridge, pp. 427–554.
- Persico, D., Villa, G., 2004. Eocene–Oligocene calcareous nannofossils from Maud Rise and Kerguelen Plateau (Antarctica): paleoecological and paleoceanographic implications. *Mar. Micropaleontol.* 52, 153–179.
- Popov, S.V., Rögl, F., Rozanov, A.Y., Steininger, F.F., Sherba, I.G., Kovac, M., 2004. Lithological–Palaeogeographic maps of Paratethys, 10 maps Late Eocene to Pliocene. *Courier Forschungsinstitut Senckenberg* 250, pp. 1–46.
- Poros, Z., Mindszenty, A., Molnár, F., Pironon, J., Györi, O., Ronchi, P., Szekeres, Z., 2012. Imprints of hydrocarbon-bearing basinal fluids on a karst system: mineralogical and fluid inclusion studies from the Buda Hills, Hungary. *Int. J. Earth Sci.* 101, 429–452.
- Premoli Silva, I., Jenkins, D.G., 1993. Decision on the Eocene–Oligocene boundary stratotype. *Episodes* 16, 379–382.
- Price, G.D., Sellwood, B.W., Corfield, R.M., Clarke, L., Cartledge, J.E., 1998. Isotopic evidence for palaeotemperatures and depth stratification of Middle Cretaceous planktonic foraminifera from the Pacific Ocean. *Geol. Mag.* 135, 183–191.
- Rögl, F., 1998. Palaeogeographic considerations for Mediterranean and Paratethys Seaways (Oligocene to Miocene). *Ann. Naturhist. Mus. Wien* 99, 279–310.
- Rosignol-Strick, M., Nesteroff, W., Olive, P., Vergnaud-Grazzini, C., 1982. After the deluge: Mediterranean stagnation and sapropel formation. *Nature* 295, 105–110.
- Salamy, K.A., Zachos, J.C., 1999. Latest Eocene–Early Oligocene climate change and Southern Ocean fertility: inferences from sediment accumulation and stable isotope data. *Paleoogeogr. Palaeoclimatol. Palaeoecol.* 145, 61–77.
- Scherbacher, M., Schmiedl, G., Hemleben, C., 2001. Early Oligocene benthic Foraminifera from the Lower Inn Valley area: implications for the paleoenvironmental evolution of the Inneralpine Molasse. In: Piller, W.E., Rasser, M.W. (Eds.), *Paleogene of the Eastern Alps*. Österreichischen Akademie der Wissenschaften Schriftenreihe der erdwissenschaftlichen Kommission, Wien, pp. 611–640.
- Schiebel, R., 1992. Recent benthic foraminifera in sediments of the shelf and upper continental slope from the Gulf of Guinea (West Africa). *Berichte-Reports, Institute of Geology and Palaeontology, University of Kiel* 51, pp. 1–179.
- Schmiedl, G., Mackensen, A., Müller, P.J., 1997. Recent benthic foraminifera from the eastern South Atlantic Ocean: dependence on food supply and water masses. *Mar. Micropaleontol.* 32, 249–287.
- Schmiedl, G., Scherbacher, M., Bruch, A., Jelen, B., Nebelsick, J.H., Hemleben, C., Mosbrugger, V., Rifej, H., 2002. Paleoenvironmental evolution of the Paratethys in the Slovenian Basin during the Late Paleogene. *Int. J. Earth Sci.* 91, 123–132.
- Schmiedl, G., Mitschele, A., Beck, S., Emeis, K.-C., Hemleben, C., Schulz, H., Sperling, M., Weldeaba, S., 2003. Benthic foraminiferal record of ecosystem variability in the eastern Mediterranean Sea during times of sapropel S5 and S6 deposition. *Paleoogeogr. Palaeoclimatol. Palaeoecol.* 190, 139–164.
- Sexton, P.F., Wilson, P.A., Pearson, P.N., 2006. Microstructural and geochemical perspectives on planktic foraminiferal preservation: “Glassy” versus “Frosty”. *Geochem. Geophys. Geosyst.* 7, Q12P19.
- Shackleton, N.J., Kennett, J.P., 1975. Paleotemperature history of the Cenozoic and the initiation of Antarctic glaciation: oxygen and carbon isotope analyses in DSDP Sites 277, 279, and 281. *Initial Rep. Deep Sea Drill. Proj.* 29, 743–755.
- Spötl, C., Venemann, T.W., 2003. Continuous-flow IR-MS analysis of carbonate minerals. *Rapid Commun. Mass Spectrom.* 17, 1004–1006.
- Tang, C.M., Stott, L.D., 1993. Seasonal salinity changes during Mediterranean sapropel deposition 9000 years B.P.: evidence from isotopic analyses of individual planktonic foraminifera. *Paleoceanography* 8, 473–493.

- Tari, G., Báldi, T., Báldi-Beke, M., 1993. Paleogene retroarc flexural basin beneath the Neogene Pannonian Basin: a geodynamic model. *Tectonophysics* 226, 433–455.
- Thierstein, H.R., Young, J.R. (Eds.), 2004. *Coccolithophores: From Molecular Processes to Global Impact*. Springer, Berlin, Heidelberg (569 pp.).
- Vető, I., Ozsvárt, P., Futó, I., Hetényi, M., 2007. Extension of carbon flux estimation to oxic sediments based on sulphur geochemistry and analysis of benthic foraminiferal assemblages: a case history from the Eocene of Hungary. *Palaeogeogr. Palaeoclimatol. Palaeoecol.* 248, 119–144.
- Violanti, D., Lozar, F., Natalicchio, M., Dela Pierre, F., Bernardi, E., Clari, P., Cavagna, S., 2013. Stress-tolerant microfossils of a Messinian succession from the Northern Mediterranean basin (Pollenzo section, Piedmont, northwestern Italy). *Boll. Soc. Paleontol. Ital.* 52, 45–54.
- Vörös, A., 1989. Middle Eocene transgression and basin evolution in the Transdanubian Central Range, Hungary: sedimentological contribution. *Fragmenta Mineral. Palaeontol.* 14, 63–72.
- Winter, A., Siesser, W.G., 1994. *Coccolithophores*. Cambridge University Press, Cambridge (229 pp.).
- Zachos, J.C., Stott, L.D., Lohmann, K.C., 1994. Evolution of marine temperatures during the Paleogene. *Paleoceanography* 9, 353–387.
- Zachos, J.C., Quinn, T.M., Salamy, K.A., 1996. High-resolution (104 years) deep-sea foraminiferal stable isotope records of the Eocene-Oligocene climate transition. *Paleoceanography* 11, 251–266.
- Zachos, J.C., Pagani, M., Sloan, L., Thomas, E., Billups, K., 2001. Trends, rhythms, and aberrations in global climate 65 Ma to present. *Science* 292, 683–693.
- Zanazzi, A., Kohn, M.J., MacFadden, B.J., Terry, D.O., 2007. Large temperature drop across the Eocene-Oligocene transition in Central North America. *Nature* 445, 639–642.
- Ziegler, P.A., 1990. *Geological Atlas of Western and Central Europe*, second ed. Shell International Petroleum Maatschappij B.V., The Hague (239 pp.).